https://doi.org/10.5194/bg-2020-84
Preprint. Discussion started: 9 April 2020

Biogeosciences Discussions
Open Access
EGU

Elevated sources of cobalt in the Arctic Ocean

Randelle M. Bundy[1,a,*], Alessandro Tagliabue[2], Nicholas J. Hawco[1,4], Peter L. Morton[3], Benjamin S. Twining[4], Mariko Hatta[5], Abigail Noble[1,b], Mattias R. Cape[1,a], Seth G. John[6], Jay T. Cullen[7] and Mak A. Saito[1]

[1]Department of Marine Chemistry and Geochemistry, Woods Hole Oceanographic Institution, Woods Hole, MA, USA
[2]School of Environmental Sciences, University of Liverpool, Liverpool, United Kingdom
[3]National High Magnetic Field Laboratory, Tallahassee, FL, USA
[4]Bigelow Laboratory for Ocean Sciences, East Boothbay, ME, USA
[5]Department of Oceanography, University of Hawai'i at Manoa, Honolulu, HI
[6]Department of Earth Sciences, University of Southern California, Los Angeles, CA, USA
[7]School of Earth and Ocean Sciences, University of Victoria, Victoria, BC, Canada
[a] School of Oceanography, University of Washington, Seattle, WA, USA
[b]California Department of Toxic Substances Control, Sacramento, CA, USA

[*]corresponding author: msaito@whoi.edu

Keywords: cobalt, GEOTRACES, Arctic Ocean, biogeochemical model

Running header: Elevated cobalt in the Arctic

https://doi.org/10.5194/bg-2020-84
Preprint. Discussion started: 9 April 2020

Biogeosciences Discussions

Abstract

Cobalt (Co) is an important bioactive trace metal that can limit or co-limit phytoplankton growth in many regions of the ocean. Total dissolved and labile Co measurements in the Canadian sector of the Arctic Ocean during U.S. GEOTRACES Arctic expedition (GN01) and the Canadian International Polar Year-GEOTRACES expedition (GIPY14) revealed a dynamic biogeochemical cycle for Co in this basin. The major sources of Co in the Arctic were from shelf regions and rivers, with only minimal contributions from other freshwater sources (sea ice, snow) and aeolian deposition. The most striking feature was the extremely high concentrations of dissolved Co in the upper 100 m, with concentrations routinely exceeding 800 pmol L^{-1} over the shelf regions. This plume of high Co persisted throughout the Arctic basin and extended to the North Pole, where sources of Co shifted from primarily shelf-derived to riverine, as freshwater from Arctic rivers was entrained in the Transpolar Drift. Dissolved Co was also strongly organically-complexed in the Arctic, ranging from 70-100% complexed in the surface and deep ocean, respectively. Deep water concentrations of dissolved Co were remarkably consistent throughout the basin (~55 pmol L^{-1}), with concentrations reflecting those of deep Atlantic water and deep ocean scavenging of dissolved Co. A biogeochemical model of Co cycling was used to support the hypothesis that the majority of the high surface Co in the Arctic was emanating from the shelf. The model showed that the high concentrations of Co observed along the transect were due to the large shelf area of the Arctic, as well as dampened scavenging of Co by manganese (Mn)-oxidizing bacteria due to the lower temperatures. The majority of this scavenging appears to have occurred in the upper 200 m, with minimal additional scavenging below this depth. Preliminary evidence suggests that both dissolved and labile Co are increasing over time on the Arctic shelf, and the elevated surface concentrations of Co likely leads to a net flux of Co out of the Arctic, with implications for downstream biological uptake of Co in the North Atlantic and elevated Co in North Atlantic Deep Water. Understanding the current distributions of Co in the Arctic will be important for constraining changes to Co inputs resulting from regional intensification of freshwater fluxes from ice and permafrost melt in response to ongoing climate change.

https://doi.org/10.5194/bg-2020-84
Preprint. Discussion started: 9 April 2020

Biogeosciences Discussions Open Access EGU

1. Introduction

Cobalt (Co) is an essential micronutrient in the ocean. It is utilized by eukaryotic phytoplankton as a substitute for zinc (Zn) in the metalloenzyme carbonic anhydrase (Lane and Morel, 2000; Sunda and Huntsman, 1995; Yee and Morel, 1996), and cyanobacteria have an absolute requirement for Co (Hawco and Saito, 2018; Saito et al., 2002; Sunda and Huntsman, 1995). Co is also the metal center in the micronutrient cobalamin, or vitamin B_{12}. In most ocean basins, dissolved Co (dCo; < 0.2 µm) is extremely scarce in surface waters (< 10 pmol L^{-1}), and is strongly complexed by a pool of thus far uncharacterized organic Co-binding ligands (Saito et al., 2005; Saito and Moffett, 2001). Due to its low concentrations and strong organic complexation, dCo has been found to be the limiting or co-limiting nutrient for phytoplankton growth in several regions (Bertrand et al., 2007, 2015; Browning et al., 2017; Martin et al., 1989; Moore et al., 2013; Saito et al., 2005). Growth limitation can be due to either a lack of dCo, or cobalamin (Bertrand et al., 2012; Bertrand et al., 2007; Browning et al., 2017), as cobalamin is only synthesized by cyanobacteria and some archaea (Doxey et al., 2015). However, many phytoplankton utilize cobalamin for the synthesis of methionine (Yee and Morel, 1996; Zhang et al., 2009), and therefore must obtain it from the natural environment (Heal et al., 2017).

Co is taken up as a micronutrient by phytoplankton in surface waters and is regenerated from sinking organic matter at depth, but it is also prone to intense scavenging throughout the mesopelagic ocean (Hawco et al., 2018; Saito et al., 2017). The strongest removal mechanism for dissolved Co (dCo) is through co-precipitation of dCo with manganese (Mn) by Mn-oxidizing bacteria, due to their similar redox properties and ionic radii (Cowen and Bruland, 1985; Moffett and Ho, 1996; Sunda and Huntsman, 1988). Several sources of Co to the ocean have been identified, including riverine (Tovar-Sánchez et al., 2004; Zhang et al., 1990), coastal sediments (Hawco et al., 2016; Noble et al., 2012; Noble et al., 2017), and to a lesser extent hydrothermal and aeolian inputs (Shelley et al., 2012; Thuróczy et al., 2010). The largest reservoirs of dCo thus far have been seen in oxygen deficient zones, likely due to a combination of low oxygen concentrations at the sediment-water interface and advection from reducing sediments, as well as enhanced regeneration in low oxygen waters (Hawco et al., 2016; Noble et al., 2012; Noble et al., 2017). These oxygen minimum zone sources of dCo exert an important control on the inventory of dCo, which is likely sensitive to small perturbations in bottom water oxygen concentrations (Hawco et al., 2018; Tagliabue et al., 2018).

It is important to understand the sources and sinks and internal cycling of dCo due to its important role as a micronutrient. However, Co has one of the most complex biogeochemical cycles of all of the trace metals. Thousands of measurements of both total dCo and weakly complexed and/or inorganic or "labile" Co (LCo) and particulate Co (pCo) now exist in the ocean, greatly improving our understanding of Co cycling and have facilitated the representation of the biogeochemical model of Co to be included in global ocean models (Tagliabue et al., 2018). Several observational zonal transects have been generated by large-scale programs including the international GEOTRACES program, among others. Large datasets now exist in the North Atlantic (Baars and Croot, 2015; Dulaquais et al., 2014a; Dulaquais et al., 2014b; Noble et al., 2017), South Atlantic (Noble et al., 2012), South Pacific (Hawco et al., 2016), Southern Ocean (Bown et al., 2011; Saito et al., 2010), and Mediterranean Sea (Dulaquais et al., 2017). While these studies document certain features in dCo distributions that are common in all

https://doi.org/10.5194/bg-2020-84
Preprint. Discussion started: 9 April 2020

basins, there exist unique, regionally specific features. For example, although several of the datasets included regions influenced by hydrothermal inputs, no significant Co feature associated with the neutrally buoyant plume was observed (Hawco et al., 2016) and only a small point source of dCo was observed in another case (Noble et al., 2016). Additionally, strong nepheloid layers were shown to be a bottom water sink for dCo (Noble et al., 2016).

Although the global coverage of Co measurements has greatly improved over the last decade, no published measurements to our knowledge have been made in the Arctic Ocean. The Arctic Ocean is arguably the most dynamic of the ocean basins, and is changing rapidly due to warmer temperatures affecting the maximal sea ice extent (Screen and Simmonds, 2010; Stroeve et al., 2012), the melting of permafrost (Jorgenson et al., 2006), and additional inputs of meltwater and river water (Johannessen et al., 2004; Serreze and Barry, 2011). The Arctic Ocean is also likely distinct in terms of Co cycling compared to other ocean basins due to its large shelf area, restricted circulation, and potentially distinct Co sources including sea ice, snow, and highly seasonal riverine inputs. The Arctic Ocean is known to have high concentrations of dissolved organic matter (DOM), which could influence the organic complexation of Co in this ocean basin. This study examined two distinct transects of dCo, LCo and one transect of pCo in the Canadian sector of the Arctic Ocean. We then used a Co biogeochemical model (Tagliabue et al., 2018) in order to interpret the role of external sources and internal cycling to the observed Co distributions, the potential of the Arctic to be a net source of Co to the North Atlantic, and to identify Co sources and sinks that may be sensitive to future changes in this rapidly changing ocean basin.

2. Methods

2.1 Sample collection and handling

2.1.1. Water column samples

Samples were collected on two expeditions in the Canadian section of the Arctic Ocean (Fig. 1). The first set of samples (n = 107) were collected on board the CCGS *Amundsen* from August 27, 2009 to September 12, 2009 in the Beaufort Sea as part of the Canadian IPY-GEOTRACES program (ArcticNet 0903; GIPY14). The second set of samples (n = 361) were collected on board the USCGC *Healy* (HLY1502) on the U.S. GEOTRACES Arctic expedition (GN01) from August 9, 2015-October 12, 2015. The Canadian GEOTRACES expedition sampled along the shelf and slope in the Beaufort Sea. The U.S. GEOTRACES expedition sailed in and out of Dutch Harbor, Alaska, and traversed across the Bering Shelf and Makarov Basin before reaching the North Pole on September 5, 2015 and returning south across the Canada Basin. Samples from the Canadian GEOTRACES expedition were collected using a trace metal rosette system fitted with 12 x 12 L GO-FLO bottles (General Oceanics), and only the dCo and LCo samples collected in the water column from this study are discussed here. All other metadata from this expedition can be found at http://www.bodc.ac.uk/geotraces/data/. Samples from the U.S. GEOTRACES expedition were collected using the U.S. GEOTRACES trace metal clean rosette outfitted with twenty-four 12 L GO-FLO bottles and a Vectran conducting hydrowire (Cutter and Bruland, 2012). Two GO-FLO bottles were triggered at each depth during the trace metal hydrocasts. One bottle was used for particulate trace metal sampling, and the other was used for all dissolved metal and macronutrient analyses. Upon recovery of the sampling system, the GO-

https://doi.org/10.5194/bg-2020-84
Preprint. Discussion started: 9 April 2020

FLO bottles were immediately brought inside a twenty-foot ISO container van. Sampling for bulk particulate trace metal samples has been described in detail elsewhere (Twining et al., 2015). Briefly, samples were filtered with 25 mm Supor 0.45 µm polyethersulfone filters mounted in Swinnex polypropylene filter holders (Twining et al., 2015). After filtering, the volume that passed through the filter was measured and a vacuum was applied to remove any remaining seawater on the filters. The filters were stored in trace metal clean centrifuge tubes and frozen at -20°C until analysis (Twining et al., 2015). Dissolved trace metal and nutrient samples were filtered with a 0.2 µm capsule filter (Acropak-200, VWR International) under pressurized filtered air (Cutter and Bruland, 2012). Samples for dCo and LCo from the Canadian GEOTRACES expedition were collected similarly, but were unfiltered. Nutrient samples were analyzed immediately on-board by the Ocean Data Facility at Scripps Institution of Oceanography. Samples for dCo were placed in two separate 60 mL Citranox-soaked (1%) and acid-cleaned low-density polyethylene (LDPE) bottles and were filled until there was no head space (Noble et al., 2012; Noble et al., 2017). One sample was used for LCo analyses and the other was used for total dCo analyses.

2.1.2 Ice hole samples

Ice hole samples were only analyzed from the U.S. GEOTRACES cruise (GN01). Seawater from ice holes for Co analyses was collected using Teflon coated Tygon tubing and a rotary pump with plastic wetted parts (IWAKI magnetic drive pump, model WMD-30LFY-115) from a hole at the station's sea ice floe. The hole was made with an ice corer (Kovacs 9 cm diameter Mak II corer), and allowed to sit undisturbed for ~ 1 hour under a canvas tent prior to sampling. Samples were collected from 1, 5 or 20 m at several sites. Seawater was filtered in-line with a 0.2 µm filter (Acropak-200 capsule filter) and dispensed into a carboy, where it was homogenized and brought back to the clean lab on board the ship. Sub-samples were taken for dCo from this carboy, and stored as described below for other water column dissolved samples. Additional details on ice hole samples can be found elsewhere (Marsay et al., 2018).

2.2 Sample storage

Total dCo and LCo samples were stored in two distinct ways. Oxygen concentrations have been found to have a significant effect on storage of dCo samples (Noble et al., 2017). Although the mechanism has not been fully explained, loss of some dCo species has been observed in the presence of oxygen on both acidified and non-acidified samples across regions with active biological gradients (Hawco et al., 2016; Noble et al., 2012; Noble et al., 2017, 2008). Since dCo and LCo analyses were not able to be performed at sea on either expedition, groups of six dCo samples from the U.S. expedition from a single cast were double-bagged and stored in a gas-impermeable plastic bag (Ampac) along with 3-4 gas-absorbing satchels (Mitsubishi Gas Chemical- model RP-3K). This outer bag was heat-sealed and samples were kept refrigerated (4°C) until analysis (Hawco et al., 2016, 2018; Noble et al., 2016). LCo samples were double-bagged and stored at 4°C until analysis. Samples were hand-carried at the termination of the GN01 expedition to Woods Hole Oceanographic Institution, and all samples were analyzed within three months. Samples from the Canadian GEOTRACES expedition (GIPY14) were collected as unfiltered samples, and were not stored in gas-impermeable bags prior to analysis, as the effects of oxygen on dCo loss were not known at the time of the expedition. It is possible

https://doi.org/10.5194/bg-2020-84
Preprint. Discussion started: 9 April 2020


Biogeosciences Discussions

there could have been some loss of dCo during the time between sample collection and analyses (approximately one year), and thus these concentrations could be underestimated. Additional discussion on how storage may have impacted these results is discussed in section *3.2.2* and *4.3*.

2.3 Reagent preparation

All reagents were prepared in acid-clean plastic bottles, and prior to analyses large batches of each reagent were made in order to have consistent reagent batches for all analyses. For dCo and LCo analyses, a 0.5 mol L^{-1} EPPS (N-(2-hydroxyethyl)piperazine-N-(3-propanesulfonic acid)) buffer and a 1.5 M $NaNO_2$ solution were prepared in Milli-Q (18 MΩ) and chelexed (Chelex-100, Biorad) to remove trace metal contaminants. Dimethylglyoxime (DMG) was prepared by first making a 10^{-3} mol L^{-1} EDTA solution in Milli-Q and adding 1.2 g of DMG. This solution was warmed by carefully microwaving at 50% power to prevent boiling, until the DMG was fully dissolved. The solution was placed on ice and left at 4°C to recrystallize overnight. The supernatant was decanted, and the remaining crystals were poured into an acid-cleaned plastic weigh boat and the remaining liquid was left to evaporate overnight in a Class-100 clean hood. Once dry, the remaining DMG was added to an Optima methanol solution for a final concentration of 0.1 mol L^{-1} DMG. A 1.5 mol L^{-1} solution of sodium nitrite was prepared by placing sodium nitrite in Milli-Q and chelexing the solution before use to remove trace metal contaminants. A Co standard solution was prepared weekly by adding 29.5 µl of a 1 mg L^{-1} Co AA standard (SPEX CertiPrep) to 100 mL of Milli-Q in a volumetric flask. For each new Co standard that was prepared during sample runs, an approximately 1 mL aliquot was saved for later analyses to ensure no variation was seen between batches. More information on reagent preparations can be found at https://www.protocols.io/researchers/randie-bundy/publications.

2.4 Dissolved and labile cobalt determinations

The dCo and LCo measurements were determined using a modified cathodic stripping voltammetry method (Saito and Moffett, 2001) for the GIPY14 samples, and a fully automated method based on Hawco et al. (2016) for the GN01 samples (Hawco et al., 2016). Measurements for both sample sets were performed using a Metrohm 663 VA stand connected to an Eco-Chemie µAutolabIII system. Peak determinations for samples collected on GIPY14 were completed as described in Noble et al. (2012). Sample automation and data acquisition for samples from GN01 was completed using NOVA 1.8 software (Metrohm Autolab), and peak determination was completed using a custom MATLAB code (see section 2.6).

The dCo samples were UV-irradiated for one hour in a temperature-controlled UV system prior to analysis to remove any strong organic ligands that may prevent DMG from effectively binding the entire dCo pool. For the GIPY14 samples, a modified temperature controlled UV system (Metrohm 705 Digestor) was used (Hawco et al., 2016), while for GN01 samples an integrated temperature-controlled (18°C) digestor was used (Metrohm 909 Digestor). In both cases samples were placed in acid-cleaned and Milli-Q conditioned 15 mL quartz tubes. After irradiation, 11 mL of each sample was placed into acid-cleaned and sample-rinsed 15 mL polypropylene tubes. For GIPY14 samples a final concentration of 353 µmol L^{-1} DMG and 3 mmol L^{-1} EPPS was added to each sample before analysis (Noble et al., 2016), and for GN01 samples a final concentration of 400 µmol L^{-1} DMG and 7.6 mmol L^{-1} EPPS was added to each sample before

https://doi.org/10.5194/bg-2020-84
Preprint. Discussion started: 9 April 2020

analysis. Samples were then inverted several times before either being analyzed individually or being placed on the autosampler (Metrohm 858 Sample Processor). For autosampler analyses, the system was flushed with Milli-Q and 2 mL of sample were used to condition the tubing and the Teflon analysis cup. Then 8.5 mL of sample was dosed into the cup automatically by a Dosino 800 burette (Metrohm), along with 1.5 mL addition of 1.5 M $NaNO_2$ for a final analysis volume of 10 mL. Samples were purged for 180 s with N_2 (high purity, > 99.99%) and conditioned at -0.6 V for 90 s. The inorganic Co in the sample that was complexed by DMG ($\log K^{cond} = 11.5 \pm 0.3$) forms a bis-complex with Co^{2+} that absorbs to the hanging mercury drop electrode (Saito and Moffett, 2001). The Co^{2+} and the DMG are both reduced at the electrode surface using a fast-linear sweep (from -0.6 V to -1.4 V at 10 V s^{-1}) and the height of the $Co(DMG)_2$ reduction peak that appears at -1.15 V is proportional to the dCo concentration in the sample. The dCo was quantified by triplicate scans of the sample, followed by four standard additions of either 25 or 50 pmol L^{-1} per addition that were dosed directly into the Teflon analysis cup. The slope of the linear regression of these additions and triplicate "zero" scans were used to calculate the individual sample-specific sensitivity (nA $pmol^{-1}$ L^{-1}). The average of the three "zero addition" scans was then divided by the sensitivity and then corrected for the volume of the reagent, and the blank (see section 2.5). In between sample batches, or before analyzing LCo samples, the entire auto-sampling system was rinsed with 10% HCl and then Milli-Q.

LCo measurements were made similarly to the dCo measurements, with the following amendments. LCo samples were not UV-irradiated, and 400 µmol L^{-1} DMG was added to 11 mL of sample and was equilibrated for at least 8 hours (overnight) in conditioned 15 mL polypropylene tubes. Immediately prior to placement of the sample on the autosampler, EPPS was added and the samples were analyzed as described above for dCo analyses. LCo measurements are thus operationally defined as the fraction of dCo that is labile to 400 µmol L^{-1} DMG over the equilibration period (Hawco et al., 2016; Noble et al., 2012).

2.5 Blanks and standards

The blank was prepared by UV-irradiating low dCo seawater for one hour. After UV-irradiation, the seawater was passed slowly through a Chelex-100 column to remove any metals. The clean seawater was then UV-irradiated a second time before being analyzed.

The blank used for GIPY14 samples was analyzed at the beginning and the end of the sample analyses to ensure the blank was consistent between runs. GEOTRACES consensus reference materials were also analyzed along with GIPY14 samples, the results of which are reported elsewhere (Noble et al., 2016).

For the GN01 samples, enough seawater was prepared in order to use the same blank seawater for all of the subsequent sample analyses and the blank was analyzed regularly with each batch of samples (every 10-20 samples). A combination of consensus reference materials and an in-house seawater consistency standard were used throughout the sample analyses (Table 1). SAFe and GEOTRACES standards were analyzed to ensure the accuracy of the sample measurements, and were slowly neutralized drop wise with 1 N ammonium hydroxide (Optima, Fisher Scientific) until reaching a pH of approximately 8. Aliquots of the SAFe and GEOTRACES

https://doi.org/10.5194/bg-2020-84
Preprint. Discussion started: 9 April 2020

samples were then placed in conditioned quartz tubes and UV-irradiated for one hour, before being analyzed as described above for dCo measurements. The consistency standard was prepared by UV-irradiating 2 L of Southern Ocean trace metal clean seawater as described above and was analyzed with each batch of samples to ensure consistency between sample runs.

2.6 Dissolved and labile cobalt data processing

Peak heights for the dCo and LCo samples for the GIPY14 dataset were determined in NOVA 1.8 software (Noble et al., 2016). All dCo and LCo peaks from the GN01 dataset were calculated using custom MATLAB code available on GitHub (https://github.com/rmbundy/voltammetry). Text files of the data output from NOVA 1.8 software were saved automatically from each scan, and processed in MATALB to determine the dCo and LCo peak heights. The signal was smoothed using the Savitzky-Golay smoothing function (span 5, degree 3), and the first derivative of the voltammetric signal between -1.4 and -1.1 V was calculated in order to find the start and end of the $Co(DMG)_2$ peak. The baseline was drawn and linearly interpolated between the start and the end of the peak. The final peak height was determined by finding the maximum of the signal and subtracting it from the baseline. Peak heights from the "zero addition" scans were plotted along with the standard additions, and a linear regression was computed from all seven scans. Data was flagged if the r^2 of the slope was < 0.97, and samples were re-analyzed.

2.7 Dissolved and particulate manganese measurements

The 0.2 µm-filtered seawater samples for dissolved manganese (dMn) were acidified to pH 2 using sub-boiling distilled HCl. The filtered subsamples were drawn into acid pre-washed 125 mL polymethylpentene bottles after three sample rinses, and the sample bottles were stored in polyethylene bags in the dark at room temperature before analyses, which was usually within 24 h of collection. Prior to analysis, samples for manganese (dMn) were acidified by adding 125 µL sub-boiling distilled 6 N HCl. Since the samples were determined dissolved iron (dFe) as well, the obtained samples were then microwaved in groups of 4 for 3 min in a 900 W microwave oven to achieve a temperature of 60±10°C in an effort to release dFe from complexation in the samples. Samples were allowed to cool for at least 1 h prior to flow injection analysis. dMn were determined in the filtered, acidified, microwave-treated subsamples using shipboard flow inject ion analysis (FIA) method (Resing and Mottl, 1992). Samples were analyzed in groups of 8, and the samples collected at each station were generally analyzed together during the same day. A 3-minute pre-concentration of sample (~9 ml) onto an 8-hydroxyquinoline (8-HQ) resin column yielded a detection limit of 0.55 nmol L^{-1} and a precision of 1.16% at 2.7 nmol L^{-1}.

Particulate trace element concentrations were determined through a total digestion procedure as described in Ohnemus et al. (2014) and Twining et al. (2015). Briefly, approximately 7 L of contamination-free seawater were filtered directly from Teflon-coated GO-Flo sampling bottles over acid-washed 47-mm (shelf stations) or 25-mm (open basin stations) PES Supor filters. Filters were divided in half, and one half was digested for 3 hours at 100-120°C in sealed Teflon vials containing 4 M HCl, 4 M HNO_3, and 4 M HF (Fisher Optima), which digests the marine suspended particulate matter (SPM) but leaves the PES filter mostly intact. The PES filters were rinsed with ultrahigh purity water (18.2 MΩ cm^{-1}) and removed from the digestion vials, and 60 µL of sulfuric acid (Optima) and 20 µL of hydrogen peroxide (Fisher Optima) were added to the

https://doi.org/10.5194/bg-2020-84
Preprint. Discussion started: 9 April 2020

vials to digest any filter fragments. The digest solution was taken to dryness at ~210°C (8-24 hours). The digest residue was re-dissolved in 4 mL of 0.32 M HNO_3 before measuring the total particulate Co, Mn and phosphorous (pCo, pMn, pP) concentrations by inductively coupled plasma mass spectrometry (ICP-MS; Thermo Element 2, National High Magnetic Field Laboratory, Tallahassee, Florida). Major and trace element concentrations were calibrated using an external multi-element standard curve and corrected for instrument drift using a 10-ppb indium internal standard (Twining et al., 2019).

2.8 Biogeochemical modeling of Co in the Arctic

Modeling runs in the Arctic Ocean were completed using a previously published biogeochemical model for Co (Tagliabue et al., 2018). Briefly, the Co model is part of the PISCES-v2 model and has an additional six tracers for Co, including dCo, scavenged Co (associated with Mn oxides), Co within in diatoms, Co in nanoplankton, small particulate organic Co, and large particulate organic Co (Tagliabue et al., 2018). The PISCES model is an excellent platform for these studies as it has a detailed representation of ocean biogeochemical cycling and has been used for a range of different studies. Measured pCo is equal to the sum of all of the particulate Co tracers in the model (including living and non-living pools). Excretion of Co is also simulated in a similar manner as iron (Fe) in PISCES-v2, with a fixed Co/C ratio in both mico- and meso-zooplankton that sets the excretion of dCo as a function of the Co content of their food (Tagliabue et al., 2018). The background biogeochemical model presented in Tagliabue et al. (2018) was modified slightly for this work, most notably an improved particle flux scheme (Aumont et al., 2017), with the Co specific parameterizations left unchanged. We used the model to assess the role of different processes by conducting sensitivity tests whereby the sedimentary Co source was eliminated, the riverine Co source was eliminated, the slowdown of Co scavenging at lower oxygen was removed (meaning oxygen did not affect Co scavenging) and the change in Co scavenging due to variations in bacterial biomass was instead set to a constant value. By comparing the results of these four sensitivity experiments to the control model, we were able to quantify the relative contributions of different external sources and internal cycling process.

3. Results

3.1 Oceanographic context

The Arctic Ocean is a unique ocean basin. The surface circulation in the Arctic is characterized by a clockwise current that entrains shelf water from the Chukchi and Eurasian shelfs, before being swept across the North Pole by the Transpolar Drift (TPD; Fig. 1). This current is distinguished by its low salinity and elevated concentrations of dissolved organic carbon (DOC) (Klunder et al., 2012; Wheeler et al., 1997). The Arctic Ocean is a highly stratified system, with little mixing between the major water masses (Steele et al., 2004). The major water masses that enter the Arctic through the Bering Strait are the upper modified Pacific water (mPW) and the Pacific halocline water (PHW). The mPW includes inputs from the Bering shelf, as well as freshwater inputs from rivers, sea ice melt, and glacially modified waters. PHW includes some influences from Bering Sea water (BSW; including both summer and winter water (Steele et al., 2004)). Atlantic water (AW) comprises the bulk of the intermediate and deep waters of the Arctic basin. These major water masses (mPW, PHW, AW) can be distinguished from the high-

https://doi.org/10.5194/bg-2020-84
Preprint. Discussion started: 9 April 2020

resolution nutrient, oxygen and salinity data from the conventional CTD rosette stations in the sampling region (Fig. 2). The mPW is characteristic of low salinity ($31 < S < 32$) and nutrients (Fig. 2), and contains contributions from Alaskan Coastal Water (Steele et al., 2004), as well as other modified water masses from the shelf. The PHW can be clearly identified from the elevated macronutrient concentrations (Fig. 2D), that extend from both shelf regions, but do not quite reach the stations in the vicinity of the North Pole (stations 27-37). PHW can be identified both by its elevated nutrient concentrations, as well as a temperature maximum within the salinity range of 31-33 (Steele et al., 2004; Steele and Boyd, 1998) (Fig. 2A, C). The AW comprises a relatively uniform deep layer throughout the entire Arctic basin. AW enters the Arctic through the Fram Strait and Barents Sea and cycles in a cyclonic direction around the Eurasian Basin and Canadian Basin (Aagaard and Carmack, 1989; Carmack et al., 1995) and is characterized by higher salinities (> 33), its temperature (~ -1.0°C) and lower nutrient concentrations (silicate < 5 µmol L^{-1}).

3.2 Dissolved cobalt distributions

3.2.1 Dissolved cobalt standards and blanks

Blank and consensus values for the GIPY14 dataset are reported elsewhere (Noble et al., 2016). The dCo blank for the GN01 analyses was 2.5±0.7 pmol L^{-1} (n = 29), with a corresponding limit of detection of 2.1 pmol L^{-1} (3 times the standard deviation of the blank; Table 1). To address consistency between runs an internal standard was measured (n = 26) and showed little variation amongst analyses (Table 1). Several consensus standards were also analyzed yielding results that were consistent with reported values (SAFe D1 = 47.9±2.1 (n = 3), SAFe D2 = 45.2±2.1 (n = 3), GSP = 2.4±1.8 (n = 3), and GSC = 77.9±2.8 (n = 3); Table 1).

3.2.2 Elevated dissolved cobalt in surface waters

The dCo profiles in the Arctic resembled a "scavenged-like" profile throughout the majority of the transect and were distinct from recent U.S. GEOTRACES efforts in the North Atlantic (Noble et al., 2016) and Eastern Tropical South Pacific (Hawco et al., 2016; Fig. 3). When median dCo concentrations from this study are binned by depth, the upper 50 m in the Arctic contains a median dCo concentration approximately 10 times higher than that of surface waters in the North Atlantic or South Pacific (Dulaquais et al., 2014; Hawco et al., 2016; Noble et al., 2017, 2012). Profiles in the Arctic also show no perceptible mid-depth maximum analogous to either the Atlantic or Pacific (Fig. 3), and instead dCo concentrations rapidly decline until reaching values of approximately 50-60 pmol L^{-1}. These concentrations in deep waters are slightly lower than the deep Atlantic and closer to background Pacific levels (~30-40 pmol L^{-1}).

The dCo distributions were highly elevated in surface waters (< 100 m) in the shelf regions (Fig. 4A-C, P-R) and these high concentrations persisted out into the basin in the vicinity of the North Pole (Fig. 4F-H). In the Bering Sea, dCo in surface waters ranged from 131-156 pmol L^{-1} in the upper 40 m, with an apparent surface or sub-surface minimum associated with biological drawdown (Fig. 4A). Concentrations significantly increased in stations near the Bering Strait (stations 2-6; Fig. 4B), where dCo reached up to 457 pmol L^{-1} in surface waters (Fig. 4B; Fig. 5), and was even higher in bottom waters, sometimes exceeding 1.5 nmol L^{-1} (Fig. 4B; Fig. 5). Surface enrichment of dCo was even more pronounced on the Chukchi shelf, where

https://doi.org/10.5194/bg-2020-84
Preprint. Discussion started: 9 April 2020


Biogeosciences Discussions

concentrations consistently exceeded 800 pmol L^{-1} (Fig. 4Q; Fig. 5). The dCo and LCo concentrations from the Canadian GEOTRACES expedition in 2009 also had near surface maxima in dCo and LCo, with up to 300 pmol L^{-1} dCo (Fig. 4R). These concentrations were lower than nearby samples collected in 2015 (Fig. 4P, Q), which contained up to three times more dCo in the upper 100 m.

The elevated dCo concentrations on both shelves traversed by the U.S. expedition persisted throughout the marginal ice zone (MIZ; stations 12-17, 51-54) and into the Canada basin (stations 12-26), following similar patterns in dFe and dMn (L. Jensen and M. Hatta pers. comm.). Some high concentrations of dCo were observed in the region of the MIZ and in samples with pronounced influence from meltwater (> 1.5% sea ice melt; Table 2) in the upper 30 m, with median dCo concentrations equal to 357.5 pmol L^{-1} in the MIZ, though with large variability (range 25.9-546.2 pmol L^{-1}) likely due to surface drawdown and additional dCo sources. Surface concentrations in this region ranged from approximately 100-500 pmol L^{-1} (Fig. 4D-F, M-N). The dCo in surface waters decreased slightly in the Makarov Basin and reached some of the lowest observed concentrations at the North Pole (210 pmol L^{-1}; Fig. 4H; Fig. 5), though concentrations were still slightly higher than at Station 1, the only Pacific station (Fig. 4A). Although some elements such as dFe showed noticeable elevated concentrations in the vicinity of North Pole in surface waters compared to surrounding waters (L. Jensen, pers. comm.), dCo remained lower than on the shelf and in the MIZ (Fig. 5). Surface dCo at the North Pole was approximately 250 pmol L^{-1}, nearly half the concentrations observed in the Canada Basin (Fig. 4H).

3.2.3 Dissolved cobalt in Pacific halocline and deep waters

While silicate (SiO_3) and phosphate (PO_4^{3-}) concentrations were indicative of the advection of PHW (Fig. 2E, F), dCo did not show a prominent enhancement within this feature (Fig. 5A), likely due to the slightly lower relative concentrations of dCo in Pacific waters compared to shelf waters (station 1; Fig. 4A). Median concentrations of dCo in waters dominated by Pacific water (> 95%) were 269.6 pmol L^{-1} (range 64.1-687.3 pmol L^{-1}) while on the shelf they were 526.0 pmol L^{-1} (Table 2). Any elevated dCo concentrations observed within the PHW density layer (σ_θ= 26.2-27.2; Steele et al., 2004) was likely added along the flow path of Pacific water across the Bering Shelf (Fig. 4B). Thus, stronger relationships were observed with other elements which are also elevated on the shelf (e.g. dFe and dMn; M. Hatta pers. comm.) than with SiO_3 or other macronutrients (e.g. PO_4^{3-}).

The dCo was remarkably constant within the deep Arctic, reflective of both AW and deep Arctic bottom water (Fig. 5A; Swift et al., 1983). Concentrations in AW (> 95% AW, and all depths > 500 m) had a median value of 61.6 pmol L^{-1} (Table 2), in between the average deep water dCo concentrations found in the Pacific and Atlantic (Fig. 3). The near-bottom sample from some profiles also showed slightly lower dCo (< 5 pmol L^{-1}) than the sample immediately above it (Fig. 4C, D, F), perhaps indicating some influence of the weak nepheloid layers on bottom-water scavenging of dCo in the Arctic (Noble et al., 2016).

3.3 Labile cobalt distributions

https://doi.org/10.5194/bg-2020-84
Preprint. Discussion started: 9 April 2020


Biogeosciences Discussions

444 *3.3.1 Labile cobalt in surface waters*
445
446 LCo is the fraction of total dCo that is either not organically complexed or weakly bound by
447 organic ligands, and represents the "labile" fraction of the total dCo pool either in terms of
448 biological uptake or scavenging (Saito et al., 2004; Saito and Moffett, 2001). LCo distributions
449 looked remarkably similar to dCo in the upper water column (Fig. 4, 5). Concentrations were
450 lower than dCo, ranging from 0 (not detectable) to 600 pmol L^{-1} on the Canadian side of the
451 Chukchi Shelf (station 61, 66). LCo comprised 20-35% of the total dCo pool in the upper water
452 column (Fig. 6), with the highest percentage of LCo found over the Chukchi shelf and
453 approximately 20% LCo in Pacific waters (station 1; Fig. 6). LCo decreased more rapidly with
454 respect to distance from the shelf than dCo in the Canada Basin and towards the North Pole, with
455 the North Pole region containing significantly lower median concentrations of LCo (10.3 pmol L^{-1}, $p < 0.05$) than surrounding waters (148.0 and 117.0 pmol L^{-1} on the shelf and MIZ,
457 respectively; Table 2). The majority of the LCo appeared to either be removed via scavenging or
458 biological uptake in the upper water column in the Canada Basin and along the Lomonosov
459 Ridge. Some of the highest median LCo concentrations were observed in the upper 30 m in the
460 MIZ and in waters containing significant sea ice melt (> 1.5%, Table 2), with median
461 concentrations rivaling those on the shelf (Table 2). The LCo in these samples had a large range
462 in many cases (48.8-233.0 pmol L^{-1} in samples with > 1.5% sea ice melt), suggesting that sea ice
463 may be a source of LCo, and that it is taken up quickly in surface waters after input from
464 meltwater.
465
466 *3.3.2 Labile cobalt in Pacific halocline waters and deep waters*
467
468 LCo was extremely low, and often undetectable, in the deep waters of the Arctic (Fig. 4). Any
469 detectable LCo at these depths represented less than 10% of total dCo (Fig. 6), with the majority
470 of the dCo in the deep Arctic was strongly organically complexed. Similar to dCo, there was no
471 observable enhancement of LCo in PHW, with LCo closely following that of dCo and other
472 shelf-enhanced trace metals such as dFe and dMn (L. Jensen, pers. comm.). LCo decreased
473 below the upper 250 m, and the median concentration of LCo in the Atlantic layer was 2.2 pmol
474 L^{-1} (Table 2) virtually equal to the detection limit of the method (2.1 pmol L^{-1}), suggesting
475 scavenging or uptake of LCo in the upper water column and little to no detectable LCo in deep
476 waters of the Arctic.
477
478 *3.4 Dissolved and particulate manganese and particulate cobalt distributions*
479
480 DCo and dMn had very similar distributions across the transect (Hatta et al. in prep). The pCo
481 and pMn concentrations were slightly decoupled from the dissolved concentrations, with a
482 subsurface peak in both (Fig. 7), as opposed to the surface peak observed in dCo and dMn (Hatta
483 et al. in prep). The maximum in pCo and pMn occurred at depths of approximately 200-300 m,
484 corresponding to a region of significantly elevated concentrations of particulate Mn-oxides (P.
485 Lam pers. comm.). Overall, pCo and pMn concentrations were the highest on the shelf, with
486 visible increases at the base of the profiles near the sediment water interface (Fig. 7B, C).
487 Concentrations of pCo and pMn declined by almost an order of magnitude from the shelves into
488 the Arctic basin, with concentrations ranging from 20-40 pmol L^{-1} and 1-10 nmol L^{-1} for pCo and
489 pMn, respectively. Deep water (> 1000 m) particulate concentrations for both metals were

https://doi.org/10.5194/bg-2020-84
Preprint. Discussion started: 9 April 2020

remarkably consistent, with concentrations varying slightly over the entire Arctic basin (Fig. 7D, H). These deep water pMn and pCo concentrations are notably higher than in other regions, such as deep Pacific waters (Lee et al., 2018).

3.5 Modeling sensitivity experiments

Overall, the control model agrees well with the data over a number of different depth strata (Fig. 8). In the surface layer (0-50m), the model output is most consistent with the observations (Fig. 8A), although in general, the model tends to produce maximum levels of dCo that underestimate the highest dCo concentrations observed. Part of this is likely due to the fact that we are comparing annual mean model output against synoptic scale in situ observations. However, the model may also be underestimating sources of dCo in the Arctic. Below 50 m, there is also good agreement with observations (Fig. 8B), with the model capturing the much lower dCo characteristic of these waters and in particular the contrast between our data in the Arctic and other data from the North Atlantic (Dulaquais et al., 2014). In the deepest layers (Fig. 8C and D), the model again is able to reproduce the decline in dCo to ~60 pmol L^{-1} and the consistency between the deep Arctic and North Atlantic.

In order to capture the major processes contributing to the modeled dCo sources and sinks, the proportion of the dCo signal in two distinct depth horizons was further explored using a set of sensitivity experiments. In the 0-50 m depth range (Fig. 9), rivers in the model have no large scale impact on the Arctic-wide dCo signal (Fig. 9A), while removing sediment margin sources reduced dCo by over 80%, (Fig. 9B). The strong effect of sediment Co supply in the model is largely driven by the large shelf area in the Arctic. In contrast to the eastern tropical Pacific oxygen minimum zone where low oxygen concentrations contributed significantly to the source of dCo (Tagliabue et al., 2018) due to reductive dissolution of sedimentary Mn-oxides (Hawco et al., 2016), enhanced sediment Co supply under low oxygen had no impact in the Arctic, due to higher levels of oxygen typical of this basin. Similarly, modulating the effect of oxygen on Co scavenging also had little impact in the Arctic (Fig. 9C). It was notable that keeping bacteria scavenging constant (e.g. eliminating the effect of changes in bacterial biomass on scavenging) reduced dCo at the surface by over 60% in some places, indicating that lower rates of scavenging was also contributing to the high rates of dCo in the surface ocean (Fig. 9D). Thus, our model experiments suggest that the high levels of dCo in the Arctic surface waters are due to sedimentary supply, with a secondary role played by reduced scavenging due to low rates of activity associated with Mn-oxidizing bacteria due to colder temperatures. In the 700-800 m depth horizon, we similarly find that changing sediment supply is more important than rivers (Fig. 10A and B), but that the effect of sediments is reduced compared to the surface. Equally, retardation of Co scavenging under low oxygen has a minor role in the ocean interior (Fig. 10C), with bacterial biomass again having a significant effect on the interior dCo signal (Fig. 10D). Thus in contrast with the surface, we find that in the 700-800 m stratum there is a roughly equal role played by sediment Co supply and low rates of Co removal by Mn-oxidizing bacteria in maintaining the dCo signal. These results are different to similar assessments in the southern equatorial Pacific where the lower oxygen levels typical of this region led to an enhanced role for sediment supply linked to low oxygen and reduced Co scavenging under low water column oxygen in driving high levels of dCo (Tagliabue et al., 2018).

https://doi.org/10.5194/bg-2020-84
Preprint. Discussion started: 9 April 2020

4. Discussion

4.1 Quantifying external sources of cobalt to the Arctic Ocean

The coherence of the dCo and LCo distributions with that of dMn, along with evidence from the model output, suggest that the extensive shelf sediments in the Arctic are the dominant source of Co in the Canadian section of the Arctic Ocean (Fig. 5, 9). Mn is known to be an excellent tracer of sediment input due to the high solubility of reduced Mn emanating from reducing sediments (Johnson et al., 1992; März et al., 2011; McManus et al., 2012; Noble et al., 2012). By using the dMn concentrations as a tracer for shelf input, we can quantify the proportion of the variance in the dCo and LCo observations that are explained by this proxy for shelf input. Linear regressions between dCo or LCo distributions and dMn in the upper 200 m across all of the stations explains 73% and 79% of the variance in the dCo and LCo concentrations, respectively (Fig. 11A; $p < 0.05$). This trend is driven primarily by the data in the upper 50 m. The variance explained decreases however, if only the shelf stations (stations 2-10, 57-66) are included in the analysis (data not shown), suggesting that some process other than shelf inputs couples the dMn and Co distributions within the basin. The amount of the variance in the Co distributions that is explained by shelf inputs is slightly less than that observed in the model (Fig. 9B), though both agree that shelf inputs are the dominant source.

The modeling results suggest that nearly all of the dCo in the upper 50 m can be accounted for by a combination of a sediment source and diminished scavenging (Fig. 9B and D). However, the inferences from observations suggest that 20-30% of the variance cannot be explained by a shelf source alone. If the dCo and LCo is examined against salinity for all stations in the transect in the upper 200 m, then salinity can explain 24% and 28% of the variance for dCo and LCo, respectively (data not shown). This relationship is improved if only the stations in the central Arctic basin are included (stations 30-43), and then salinity explains 47% of the dCo and 57% of the LCo distributions (Fig. 11B). The coherence of dCo and LCo with salinity across the dataset, and particularly in this region, appears to be due to a contribution of low salinity water from rivers, rather than from sea ice melt (Fig. 12C), as no relationship was observed with the fraction of sea ice melt determined from $\delta^{18}O$ isotopic measurements of seawater (Bauch et al., 2005; Cooper et al., 2005, 1997). Instead, the relationship with salinity is driven by freshwater inputs from rivers, as a strong relationship is observed with the fraction of meteoric water (Fig. 12D). These stations correspond to a region of anomalously high dFe and DOC concentrations (Jensen et al., in prep, D. Hansell, pers. comm.), interpreted to be indicative of river inputs carried across the basin in the Transpolar Drift (TPD) (Gascard et al., 2008; Klunder et al., 2012; Wheeler et al., 1997). This is supported by measurements of ^{228}Ra, which track shelf inputs throughout the Arctic due to interactions between the sediment-water exchange processes (Kipp et al., 2018; van der Loeff et al., 2018). A similar relationship was also observed with salinity in the North Atlantic, supporting the role of rivers as a source of dCo (Saito and Moffett, 2001). In our model sensitivity experiments, we found a small effect of rivers on dCo (Fig. 9A and 10A), and the Co/N river endmember in the model was similar to that measured by the Arctic Great Rivers Observatory (Holmes et al., 2018). It appears that the data suggests a larger role for rivers than what is captured by the model, which could imply that gross riverine fluxes are underestimated by our model. However it is difficult to disentangle riverine processes from other processes happening on the shelf like groundwater inputs (Charette et al., in review). It is possible that

https://doi.org/10.5194/bg-2020-84
Preprint. Discussion started: 9 April 2020


Biogeosciences Discussions Open Access EGU

there is some mixing of river and sediment dCo occurring in the coastal zone or that our global scale model is not able to properly account for the physical transport of fluvial signals into the open basin.

The presence of such high concentrations of trace elements and isotopes at the North Pole was surprising, yet several tracers indicate that this is an area significantly influenced by river and shelf input from the surrounding continents (Kipp et al., 2018; van der Loeff et al., 2018). The elevated concentrations of dCo at great distances from the continental shelf is also likely partially due to the enhanced organic complexation of dCo in TPD waters. Averaged over the entire dataset dCo is 79±13% organically complexed (21±13% labile) in the upper 200 m of the water column. However, at TPD influenced stations (stations 29-34; Charette et al. in review), dCo is 92±6% organically complexed, significantly higher than in the rest of the transect (*paired sample t*-test, $p < 0.05$). This suggests that elevated concentrations of DOC from Arctic rivers entrained in the TPD or ligands produced in-situ may play a role in stabilizing a portion of the dCo pool during transport towards the North Pole. Although the exact character of the organic dCo-binding ligands in seawater are unknown, in the Arctic it is likely that humic-like substances contribute some portion of the organic complexation observed, due to the presence of elevated colored dissolved organic matter (CDOM) in the TPD (Wheeler et al., 1997), consistent with the presence of humic substances (Del Vecchio and Blough, 2004). Despite the presence of humic substances, it seems somewhat unlikely that humics account for all of the ligands complexing dCo in this region. Our analytical method distinguishes organically-bound Co as the fraction of total dCo that is more strongly complexed than our competing ligand (DMG). The complexation of humic and fulvic-like substances with Co has been shown to be much weaker than the $Co(DMG)_2$ complex ($\log K^{cond}_{Co(HS)} \sim 8$ versus $\log K^{cond}_{Co(DMG)_2} = 11.5 \pm 0.3$; Yang and Van Den Berg, 2009). Ligands similar to those suspected to complex Co in open ocean waters of the Atlantic or Pacific could be responsible for Co stabilization in the TPD waters (Saito and Moffett, 2001). These ligands are presumed to have functional groups similar to cobalamin (vitamin B_{12}), with a Co atom tightly bound inside a corrin ring. Cyanobacteria and some archaea are known cobalamin producers (Bertrand et al., 2007; Doxey et al., 2015; Heal, 2018; Heal et al., 2017; Lionheart, 2017) and both are found in the Arctic (archaea; Cottrell and Kirchman, 2009; cyanobacteria; Waleron et al., 2007; Zakhia et al., 2008), although in very low abundance. The nature of the organic molecules binding dCo in this region will be interesting to explore further in future studies.

Overall, both the modeling results and observations agree that the dominant source of Co in the Arctic is from the extensive shelf sediments surrounding the Arctic Ocean, with additional contributions from Arctic rivers. The observations however, show that sources vary in importance in space, with sediment sources clearly dominating in stations close to the shelf, and river sources dominating in the central Arctic basin through the influence of the TPD. Whether or not shelf sediments act as a capacitor, storing and then releasing Co to overlying water, for terrestrially derived riverine sources or for Co delivered to sediments in sinking marine organic matter remains unknown. It is clear however, that the riverine source dominates the distribution observed near the North Pole where dCo and LCo concentrations remain high despite the distance from land, and that organic complexation likely plays a role in the distal transport of this dCo (Charette et al., in review).

https://doi.org/10.5194/bg-2020-84
Preprint. Discussion started: 9 April 2020


Biogeosciences Discussions

628 *4.2 Cobalt scavenging and internal cycling*
629
630 A striking feature of the dCo and LCo dataset is the vertical transition in the water column from
631 high to low Co concentrations throughout the deep Arctic (Fig. 5). The question remains whether
632 or not 1) this elevated dCo is scavenged at a shallow depth horizon, or 2) if the high dCo
633 concentrations in the surface layer (< 200 m) are simply physically isolated from deeper water
634 masses, or a combination of the two. This would suggest that the Atlantic water characteristic of
635 the deep Arctic doesn't mix with the modified surface Arctic water containing high
636 concentrations of Co. We examined both hypotheses within a modeling framework and
637 compared this to the observations. In the model, the dCo is scavenged primarily in the upper 50
638 m with almost no scavenging below 200 m (data not shown). The dCo scavenging in the model
639 is primarily controlled by Mn-oxidizing bacteria, which have a strong temperature dependence in
640 the model (Tebo et al., 2004). The cold temperatures in the majority of the Arctic prevent
641 enhanced scavenging of dCo by this mechanism in the Arctic compared to other basins (Hawco
642 et al., 2018; Saito et al., 2017; Tagliabue et al., 2018). However, relatively warmer temperatures
643 on the shallow shelves suggest that scavenging is enhanced in this region (Fig. 4), and the
644 coherence of the pCo and pMn peaks in the upper 200-250 m (Fig. 7) support this mechanism of
645 upper ocean scavenging. Evidence from ^{234}Th data shows very little (to no) particulate organic
646 carbon (POC) flux in the upper water column along this transect, however strong lateral transport
647 from the shelves to the basin was observed (Black et al. 2018). This lateral transport was
648 observed both in the upper water column and at depth, suggesting fast-moving currents through
649 the deep canyons may be significant in transporting material from the shelf into the basin (Black
650 et al. 2018). It is possible that additional scavenging of Co may occur along this flow path. Some
651 of the profiles observed in the deep basin also show evidence for deeper ocean scavenging in the
652 Atlantic water (e.g. Fig. 4E, H, P).
653
654 Additional insights on Co scavenging in this basin can be observed by exploring the dCo:
655 phosphate (P) ratios (pmol L^{-1}:µmol L^{-1}) along the transect (Fig. 13). The relationship between
656 dCo and P in the Arctic water column yields insights into biological uptake and regeneration
657 processes acting on the dCo inventory, as well as scavenging. An analysis completed by Saito et
658 al. (2017) showed that positive slopes in the dCo:P relationship were indicative of regeneration,
659 while negative slopes were indicative of biological uptake or scavenging (Saito et al., 2017). The
660 high dCo in the Arctic yields a unique dCo:P relationship compared to the North Atlantic (Fig.
661 13A; Saito et al., 2017). When dCo:P slopes ($r^2 > 0.6$) are binned according whether they are
662 positive (Fig. 13B) or negative (Fig. 13C) and then plotted with depth (Fig. 13D), a few patterns
663 are apparent. Positive dCo:P slopes are observed largely within a confined depth strata in the
664 PHW (Fig. 13D). This is not surprising, given that deep Pacific waters carry a strong
665 regeneration signal. However, at most other depths in the water column the dCo:P slopes are
666 negative, showing that scavenging is occurring to some extent throughout the water column (Fig.
667 13D). With one exception, the magnitude of the negative dCo:P slopes are greater in the upper
668 water column, supporting the model results and our interpretations of the pCo profiles that most
669 of the scavenging occurs in the upper water column but also continues to occur throughout the
670 deep Arctic.
671
672 This evidence, combined with the coinciding maxima observed in pCo and pMn, suggest that a
673 significant amount of scavenging occurs in the upper water column, but that additional

https://doi.org/10.5194/bg-2020-84
Preprint. Discussion started: 9 April 2020

scavenging continues to occur below these depths. The elevated pCo concentrations in the deep Arctic compared to other regions (Lee et al., 2018) suggest that scavenging over long timescales continue to add to the pCo pool. This mechanism likely prevents high concentrations of dCo to penetrate below the shallow modified Arctic surface water. However, it is clear that there is very little mixing between the modified surface waters, the PHW, and the deep Atlantic water in the Arctic (Steele et al., 2004). Thus, it is likely a combination of upper ocean scavenging, and little mixing between water masses, that keeps the elevated dCo and LCo confined to the surface waters in Arctic, yielding the intense scavenged-like profile of Co in this region compared to other basins (Fig. 3).

4.3 Increases in Co inventories over time in the Canadian sector of the Arctic Ocean

Samples collected on the shelf in the Beaufort Sea in 2009 in proximity to the U.S. GEOTRACES transect in 2015 (Fig. 1) had significantly lower dCo (*paired t*-test, $p < 0.05$) than shelf samples from 2015 (Fig. 14). Shelf samples for dCo from 2015 were approximately 3.5 times higher than the dCo and approximately eight times higher in LCo than in 2009 (Fig. 14C). The maximum dCo concentration measured in 2009 was 301 pmol L^{-1}, while in 2015 it was 1852 pmol L^{-1}. The dCo and LCo concentrations below 150 m agreed very well however, between the two years (Fig. 14A, B). Several factors could account for the higher dCo and LCo observed in 2015 compared to 2009. The Co samples from 2009 were unfiltered, and were not stored with gas-absorbing satchels like the samples from 2015. Recently, loss of dCo has been observed in the presence of oxygen during storage, however this loss was most pronounced for samples in low oxygen regions (Noble, 2012). The mechanism of the dCo loss is unknown and is difficult to quantify from these samples, however the waters are well oxygenated in this region (Fig. 2B) and thus the loss due to storage was likely minimal. However, we can not say for certain how much of the observed increase in dCo over time is due to a storage artifact. Previous work has shown a maximum loss of dCo of 40% after 5 months of storage (Noble, 2012). If we consider that 40% of the dCo could have been lost in the samples collected from 2009, the data from 2015 still show an increase in dCo of approximately 400%. Thus, although we can not quantify with certainty the percent increase in dCo over time in the Canadian sector of the Arctic, it is likely that it is still significant.

The increase in dCo over time in the Arctic is interesting, and has been documented for other tracers in the Arctic. Kipp et al. (2018) and van der Loeff et al. (2018) noted that ^{228}Ra has increased over time in the central Arctic. They suggest that increases in shelf and/or river inputs from thawing permafrost are the source of this elevated ^{228}Ra (Kipp et al., 2018; van der Loeff et al., 2018). A similar mechanism is likely increasing metal inventories over time on Arctic shelves. The majority of the variance (~70%) in dCo in the upper 100 m on the U.S. GEOTRACES transect could be explained by a shelf source, and the remainder was likely associated with river inputs (Fig. 11). If these sources are similar to the sources of dCo in 2009, then an increase in either a shelf or river flux could be responsible for the dramatic increase in dCo over time. There is not enough data to state whether the river dCo flux has changed over time in the Arctic, however several studies have documented an increase in river discharge over time due to increases in permafrost melt (Doxaran et al., 2015; Drake et al., 2018; Kipp et al., 2018; van der Loeff et al., 2018; Tank et al., 2016; Toohey et al., 2016). The increase in river discharge has the potential to considerably increase trace metal inventories in the future Arctic

https://doi.org/10.5194/bg-2020-84
Preprint. Discussion started: 9 April 2020

Ocean, perhaps particularly for those metals that are strongly organically complexed, thus protecting against scavenging in the estuarine mixing zone (Bundy et al., 2015). These increases in metals over time will have implications for metal stoichiometries and phytoplankton growth in a changing Arctic Ocean.

4.4 Implications of the Arctic as a net source of Co to the North Atlantic Ocean

The concentrations of dCo and LCo in this region of the Arctic are some of the highest concentrations that have been observed thus far in the ocean. In some cases, the dCo was almost ten times higher than in the low oxygen region of the Eastern Pacific (Hawco et al., 2016). Although the Arctic is considered to be a macronutrient poor system, in contrast to other oligotrophic regions the Arctic is quite enriched in micronutrients (Jensen et al., 2019; Jensen et al., in prep). These distinct nutrient ratios may have implications for Arctic phytoplankton communities, as well as communities in the North Atlantic that are influenced by inputs from the Arctic.

Arctic waters are thought to primarily exit the basin and impact the North Atlantic via the Canadian archipelago and the Fram and Davis Straits (Talley, 2008). The organic complexation and stabilization as well as the high concentrations of dCo suggest that some of this dCo might exit the Arctic and impact nutrient distributions in the North Atlantic. Noble et al. (2016) noted a plume of elevated dCo in the western portion of the U.S. GEOTRACES North Atlantic (GA03) transect that did not correspond with a signature from reducing sediments as on the North Atlantic eastern boundary. Noble et al. (2016) postulated that high dCo in Labrador Seawater (LSW) was the source of this signal, due to the presence of a corresponding signature of low silica that is characteristic of this water mass. The authors noted that the anomalously high dCo could be from elevated dCo in Arctic waters, or due to high dCo on the shelf that is picked up along the flow path of the LSW, or a combination of the two (Noble et al., 2016). Our data suggests that likely a combination of the high dCo observed in this study and additional Co entrained on the shelf in the Labrador Sea contribute to that signal, and when observed in temperature and salinity space the data supports this hypothesis (Fig. 15). The Arctic source waters that contribute to the formation of LSW have a low salinity signature, and are likely significantly modified as they exit the Canadian archipelago, Fram Strait and Davis Straits (Yashayaev and Lodor, 2017). From this data we cannot quantitatively connect the elevated dCo and LCo observed in the Arctic source waters to the LSW seen in the western Atlantic, given the complex history (e.g. transformation, mixing) of source waters in the Labrador Sea region (Le Bras et al., 2017). However it is apparent that the low salinity Arctic waters contain high Co (Fig. 15), which given the advective pathways of these water masses from the Arctic, suggests that they may act as a source of Co to lower latitude waters. Interestingly, the high dCo in the Arctic has a distinct LCo/dCo signature compared to that observed in the western North Atlantic (Fig. 15A). Due to the significant impact that Arctic shelves and rivers have on the dCo signature observed in this study, it is likely that additional Co may be added to these waters as they pass through the Canadian archipelago. Additional LCo is likely entrained in this water mass as the surface Arctic water moves through the Canadian archipelago. The fate of these waters and their Co as they exit via the Fram and Davis Straits is unknown. Constraining these Arctic endmembers and how they contribute to dCo distributions in the North Atlantic deserves further

https://doi.org/10.5194/bg-2020-84
Preprint. Discussion started: 9 April 2020

attention, as it has interesting implications for nutrient resource ratios for North Atlantic phytoplankton communities.

The possibility that elevated micronutrient concentrations from the Arctic are being exported to the North Atlantic could have interesting implications for phytoplankton nutrient utilization and community composition. DCo and dZn for example, which can be interchanged within carbonic anhydrase in some eukaryotes (Lane and Morel, 2000; Sunda and Huntsman, 1995; Yee and Morel, 1996), are elevated in the Arctic compared to the North Atlantic and South Pacific (Fig. 16A, B). The higher concentrations of both metals results in a dCo/dZn ratio that is quite similar to that observed in the North Atlantic, however the range in this ratio is large (Fig. 16C). Small changes in the sources of each of these metals could manifest as big impacts on the ratio of these micronutrients in surface waters. However, the shift in these micronutrient ratios may not impact the resulting phytoplankton quotas (Figure 16D). Despite quite different total concentrations of dCo and dZn in the Arctic compared to the North Atlantic for example, the measured quotas are quite similar (Twining et al. in prep, Figure 16D). However, if river inputs continue to increase with an increase in permafrost thawing in the warming Arctic (Jorgenson et al., 2006) and similar increases in dCo are observed over time as seen in this work, then total metal inventories in the Arctic may begin to influence the North Atlantic to a greater extent. These source changes may disproportionately affect Co compared to Zn, whose primary source was found to be from a regeneration signal on the shelf rather than from river input (Jensen et al., 2019), and whose total inventory is small compared to Zn. Understanding how future changes in metal sources in the Arctic may impact the North Atlantic or shifts in phytoplankton community structure will be important to constrain.

5. Conclusions

The unique dissolved and labile Co distributions observed in the Arctic have noteworthy implications for Arctic ecosystems and for future changes in micronutrients in the warming Arctic. Sediment and river inputs to the Arctic appear to be the dominant mechanisms for the input of dCo to the Arctic, and these elevated signals persist over a broad area of the western Arctic far from their source regions. This appears, at least in part, to be due to the relatively slow scavenging of Co in this basin that is suggested from modeling outputs to be related to the low temperatures and slower kinetics of Mn-oxide formation. The majority of this scavenging appears to happen on the shelf with an advected signal of particulate Mn and Co appearing into the Arctic basin. Co was also shown in this work to be increasing over time on the shelf in the Canadian Arctic, possibly due to increases in river inputs from thawing permafrost, though this is difficult to constrain in the present dataset. Given the significant increase in Co over time in the Arctic and the modification of low-salinity Arctic waters as they exit the Arctic into the North Atlantic and the Labrador Sea, it is difficult to determine if there is a net flux of Co out of the Arctic and into the North Atlantic, however evidence in this work suggests that the distinct Co waters of the Arctic likely impact downstream micronutrient concentrations. These impacts are likely to become increasingly important in the future, with increased warming and changes to Co sources in the Arctic basin.

6. Author contributions

https://doi.org/10.5194/bg-2020-84
Preprint. Discussion started: 9 April 2020

RMB analyzed the samples and wrote the manuscript. MRC developed the data processing code and helped write the manuscript. MAS designed the study and helped write the manuscript. AT, NJH, PLM, BST, MH, AN, SGJ, and JTC contributed data and helped write the manuscript.

7. Data availability

The data for this manuscript are available through BCO-DMO for GN01 (https://www.bco-dmo.org/project/638812) and through BODC for GIPY14 (https://www.bodc.ac.uk/geotraces/data/inventories/0903/). The dissolved and labile cobalt data for GN01 specifically is available at https://www.bco-dmo.org/dataset/722472.

8. Acknowledgements

We would like to thank the captain and crew of the USGC *Healy*, Gabi Weiss and Simone Moos for sampling, and Dawn Moran, Noelle Held and Matt McIlvin for help with sample preparations and analyses, Dr. Ana Aguilar-Islas and Dr. Robert Rember for small boat and sea-ice hole operations, the Ocean Data Facility at Scripps Institution of Oceanography for macronutrient, oxygen, and salinity measurements, S. Rauschenberg for sample collection, and P. Schlosser, R. Newton, T. Koffman, and A. Pasqualini for water mass fraction data. This work was supported by NSF-OCE #1435056 to M. Saito and S. John, as well as Woods Hole Oceanographic Institution Postdoctoral Scholar grant to R.M. Bundy and M.R. Cape. M. Hatta was supported by NSF-OCE #1439253. A. Tagliabue was supported by the European Research Council (ERC) under the European Union's Horizon 2020 research and innovation programme (Grant agreement No. 724289). PM and BT were supported by NSF-OCE #1435862 and PM was also supported by the National High Magnetic Field Laboratory (PLM). PLM is supported by the National Science Foundation through DMR-1644779 and the State of Florida. J.T. Cullen was supported by the Natural Sciences and Engineering Research Council (NSERC) of Canada and an International Polar Year (IPY) Canada grant.

https://doi.org/10.5194/bg-2020-84
Preprint. Discussion started: 9 April 2020

Table 1: Average dCo concentrations from blank, internal standard, and consensus standard runs.

	n	**dCo (pmol L^{-1})**	**std dev**
blank	29	2.5	0.7
internal standard	26	50.3	7.6
SAFe D1	3	47.9	2.1
SAFe D2	3	45.2	2.1
GSP	3	2.4	1.8
GSC	3	77.9	2.8

https://doi.org/10.5194/bg-2020-84
Preprint. Discussion started: 9 April 2020

Table 2: Median, maximum and minimum concentrations of total dissolved (dCo) and labile cobalt (LCo) in samples with representative water masses and sources in the Arctic Ocean. Median concentrations were determined in each water mass type by using water masses that contained > 95% Atlantic water, > 95% Pacific water, > 10% meteoric water, and > 1.5% sea ice melt. Shelf stations were stations 2-10 and 60-66, MIZ stations 10-17 and 51-57 (< 30 m), and North Pole stations 27-36 (< 200 m). Ice hole samples were sampled from 1 and 5 m. The notation 'nd' means not determined.

	dCo (pmol L^{-1})	**max**	**min**	***n***	**LCo (pmol L^{-1})**	**max**	**min**	***n***
Atlantic	61.6	126.3	36.9	37	2.2	5.8	0.2	27
Pacific	269.6	687.3	64.1	41	45.8	133.8	2.5	35
Meteoric	266.1	497.2	64.1	27	77.5	139.8	11.6	25
Shelf	526.0	1852.1	25.9	30	148.0	578.7	6.1	30
MIZ	357.5	546.2	25.9	19	117.0	158.6	6.1	19
North Pole	139.8	280.2	64.2	14	10.3	22.0	1.5	14
sea ice melt	526.0	1021.5	207.3	3	151.1	233.0	48.8	3
ice hole	281.1	316.2	259.4	4	nd	nd	nd	4

https://doi.org/10.5194/bg-2020-84
Preprint. Discussion started: 9 April 2020

Figure Captions

Figure 1: Standard CTD sampling stations (green) and trace metal rosette (TM) sampling stations (blue) from the GN-01 expedition in 2015, and trace metal sampling locations from the GIPY14 expedition in 2009 (red).

Figure 2: *In-situ* temperature (A), nitrate (B), salinity (C), phosphate (D), oxygen (E), and silicate (F) with neutral density anomaly contours from the northern and southern legs of the GN-01 transect as shown in Figure 1. Major water masses are labeled as modified Pacific Water (mPW), Pacific Halocline Water (PHW) and Atlantic Water (AW).

Figure 3: Median dCo concentrations at specific depth intervals from the Arctic Ocean (this study; red circles), Atlantic Ocean (blue triangles), and the Pacific Ocean (orange squares). Shaded regions indicate the upper and lower quartiles of the data in each dataset.

Figure 4: Dissolved cobalt (dCo; black circles) and labile cobalt (LCo; open circles) from all stations from the 2015 (A-Q) and 2009 (R) studies.

Figure 5: (A) dCo concentrations and (B) LCo concentrations in the Arctic Ocean.

Figure 6: The ratio of LCo (pmol L^{-1}) to total dCo (pmol L^{-1}) along the transect from south to north in the upper 1000 m.

Figure 7: Particulate manganese (pMn; open circles) and particulate cobalt (pCo; x) from several stations along the northern (A-D) and southern (E-H) legs of transect, with the same station designations as in Figure 4.

Figure 8: Model output (colors) compared to observations (dots) from 0-50 m (A), 50-150 m (B), 700-800 m (C) and 1500-2000 m (D).

Figure 9: (A) Model output of the proportion of the dCo signal from 0-50 m that is controlled by (A) rivers, (B) sediment input, (C) oxygen concentrations, and (D) removal by Mn-oxidation from Mn-oxidizing bacteria.

Figure 10: (A) Model output of the proportion of the dCo signal from 700-800 m that is controlled by (A) rivers, (B) sediment input, (C) oxygen concentrations, and (D) removal by Mn-oxidation from Mn-oxidizing bacteria.

Figure 11: dCo (closed circles) and LCo (open circles) in the upper 200 m plotted against (A) dMn in shelf stations only (stations 2-10, 57-66), as well as (B) salinity from only the stations influenced by the Transpolar Drift (stations 30-43).

Figure 12: dCo and LCo from select stations versus (A) the fraction of Atlantic water (F_{atl}; all stations < 500 m), (B) the fraction of Pacific water (F_{pac}; all stations < 500 m), (C) fraction of sea ice melt (F_{ice}; < 100 m and south of 84ºN) and (D) the fraction of meteoric water (F_{met}; < 500 m and north of 84ºN).

Figure 13: (A) The dCo (pmol L^{-1}) compared to phosphate (dP; µmol L^{-1}) from the GN01 dataset. (B) 5-point two-way linear regression of positive dCo:P slopes ($r^2 > 0.6$). (C) 5-point two-way linear regression of negative dCo:P slopes ($r^2 < -0.6$). (D) Depths where either a positive (blue) or negative (red) dCo:P slope was identified in the GN01 dataset. Additional details on the regression analysis can be found in Saito et al., (2017).

Figure 14: The dCo on the shelf measured in 2009 (GIPY14; black triangles) and 2015 (GN01; blue circles) in the upper 3500 m (A) and upper 500 m (B). Average and dCo and LCo in the upper 150 m from 2009 (grey) and 2015 (blue). Error bars represent the standard deviation and a (*) denotes a significant difference.

Figure 15: (A) The ratio of LCo to dCo (colors) from this study and the western portion of the GA03 North Atlantic transect (Noble et al., 2016) along with dCo concentrations (B) in temperature-salinity space, with Labrador Sea Water (LSW) source waters (solid black box) and

https://doi.org/10.5194/bg-2020-84
Preprint. Discussion started: 9 April 2020

882 signature in the Atlantic (dashed box) are highlighted. (C) Sampling region in this study and the
883 stations used from Noble et al. (2016).
884 **Figure 16:** Median dCo concentrations (A), dissolved Zn concentrations (B) and dCo/dZn ratios
885 (C) in the upper 200 m in the Arctic (this study), North Atlantic (Noble et al., 2016), and in the
886 Southern Eastern Pacific (Hawco et al., 2016). (D) Co/Zn ratios in phytoplankton from the Arctic
887 and North Atlantic (Twining et al., in prep). Whiskers represent the lower (25%) and upper
888 (75%) quartiles.

https://doi.org/10.5194/bg-2020-84
Preprint. Discussion started: 9 April 2020

889 **Figure 1.**

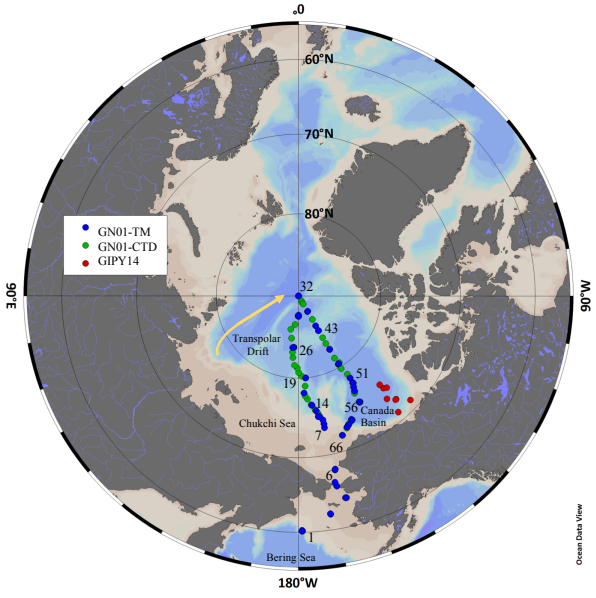

https://doi.org/10.5194/bg-2020-84
Preprint. Discussion started: 9 April 2020

890 **Figure 2.**

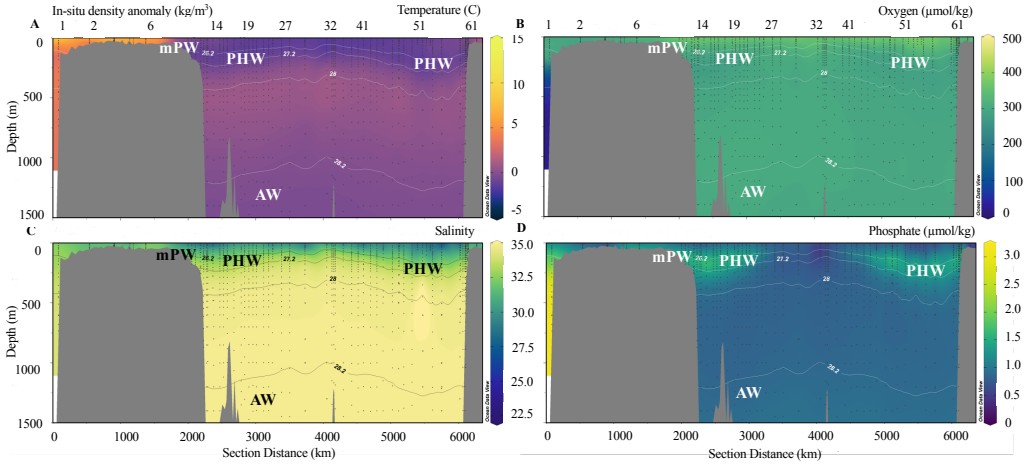

https://doi.org/10.5194/bg-2020-84
Preprint. Discussion started: 9 April 2020

891 **Figure 3.**

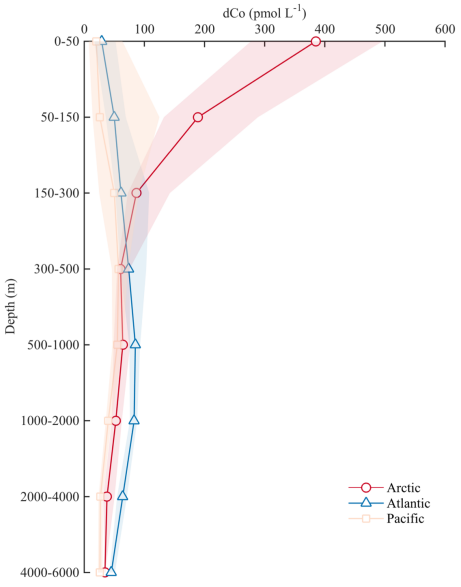

https://doi.org/10.5194/bg-2020-84
Preprint. Discussion started: 9 April 2020

892 **Figure 4.**

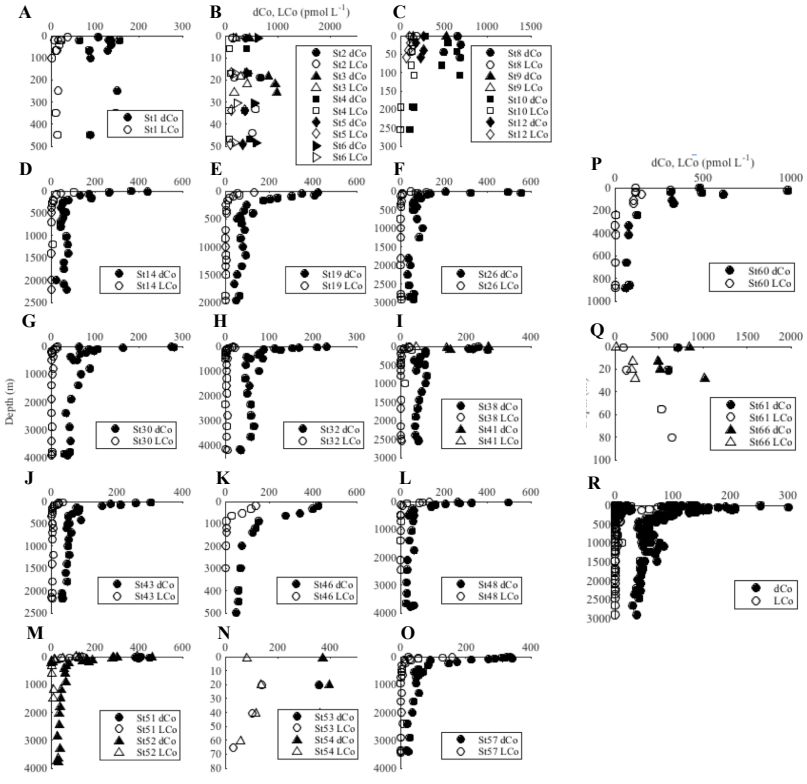

https://doi.org/10.5194/bg-2020-84
Preprint. Discussion started: 9 April 2020

893 **Figure 5.**

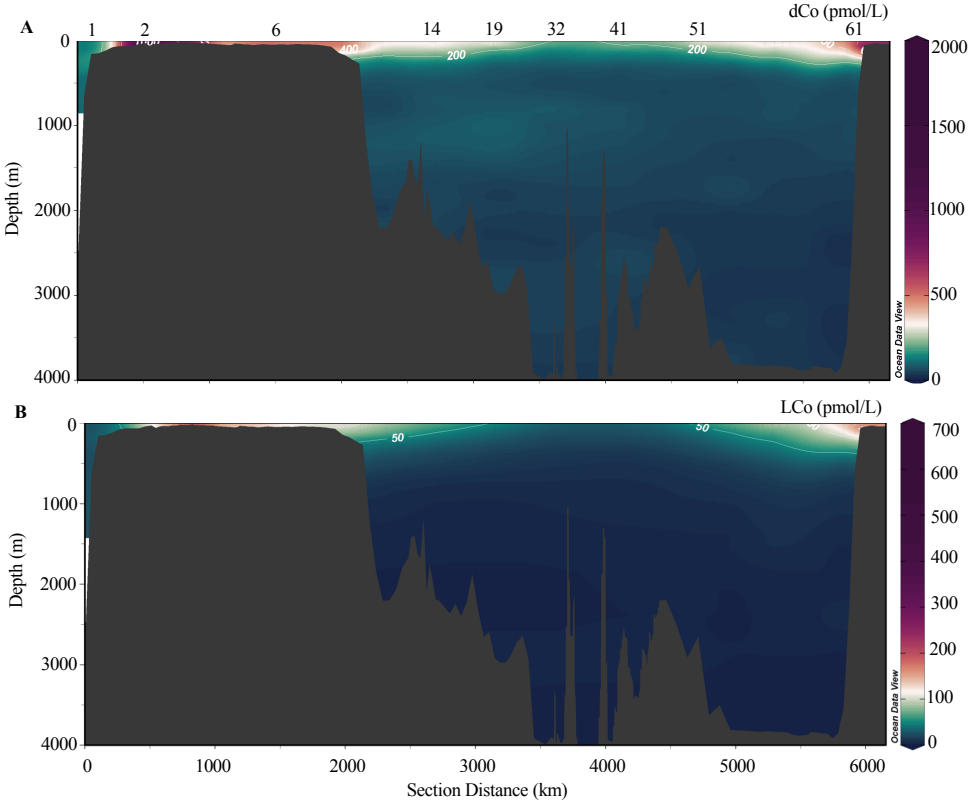

https://doi.org/10.5194/bg-2020-84
Preprint. Discussion started: 9 April 2020

894 **Figure 6.**

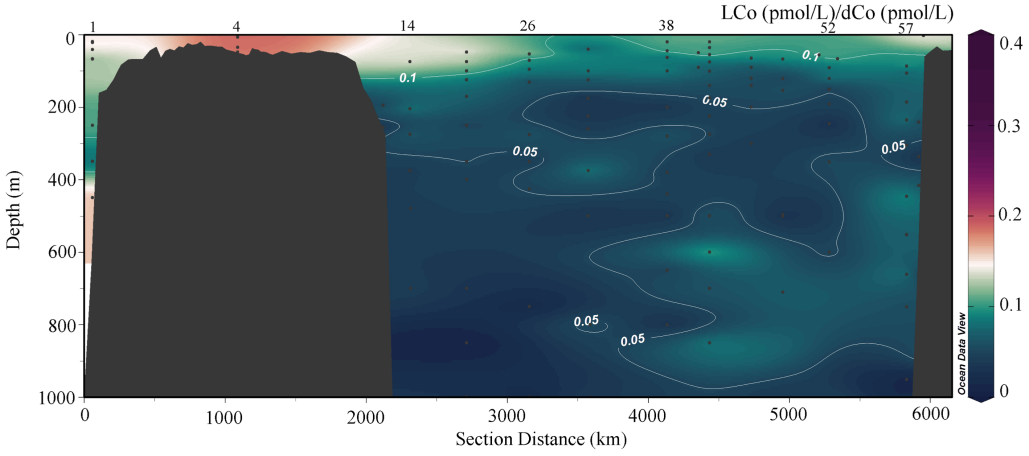

https://doi.org/10.5194/bg-2020-84
Preprint. Discussion started: 9 April 2020

Biogeosciences
Discussions
Open Access
EGU

895 **Figure 7.**

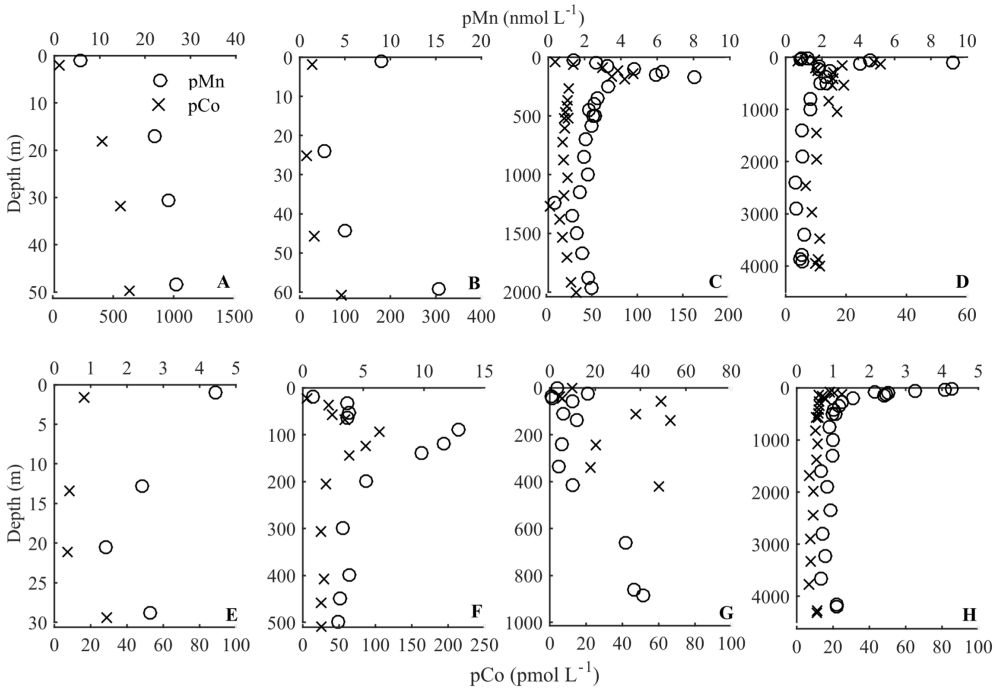

https://doi.org/10.5194/bg-2020-84
Preprint. Discussion started: 9 April 2020

Biogeosciences
Discussions
Open Access
EGU

896 **Figure 8.**

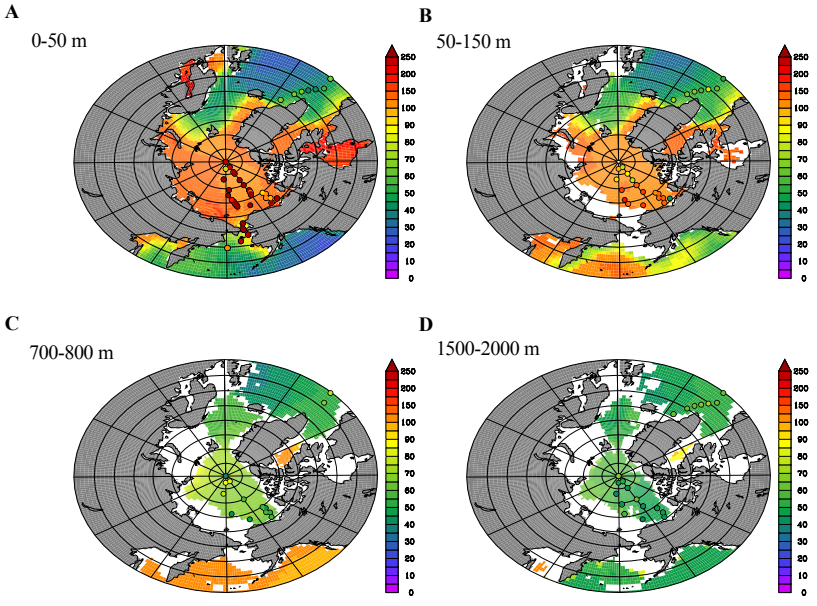

https://doi.org/10.5194/bg-2020-84
Preprint. Discussion started: 9 April 2020

897 **Figure 9.**

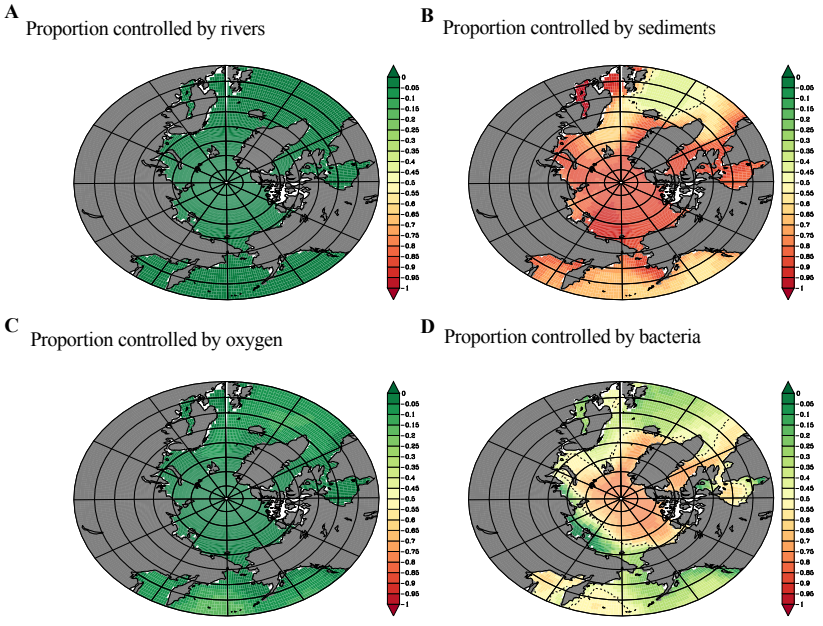

https://doi.org/10.5194/bg-2020-84
Preprint. Discussion started: 9 April 2020

Biogeosciences
Discussions
Open Access
EGU

898 **Figure 10.**

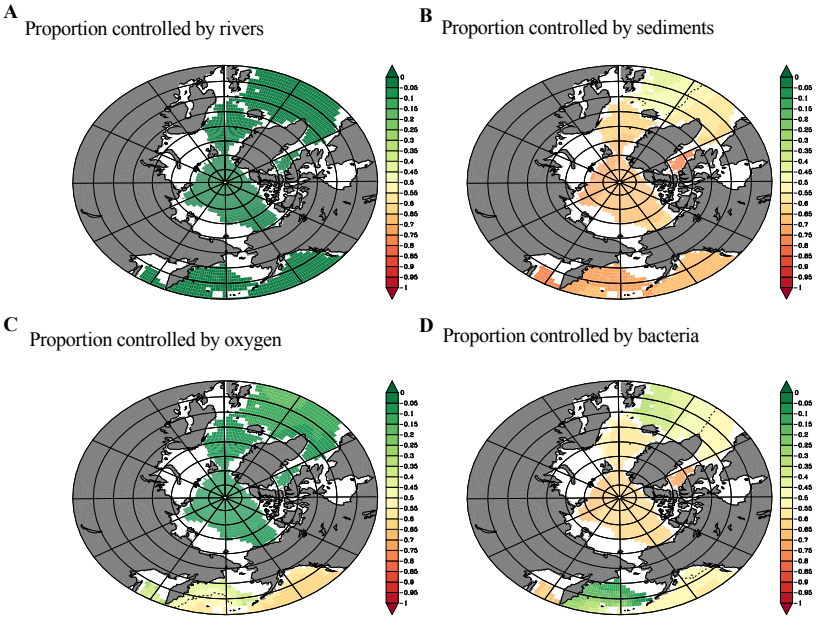

https://doi.org/10.5194/bg-2020-84
Preprint. Discussion started: 9 April 2020

899 **Figure 11.**

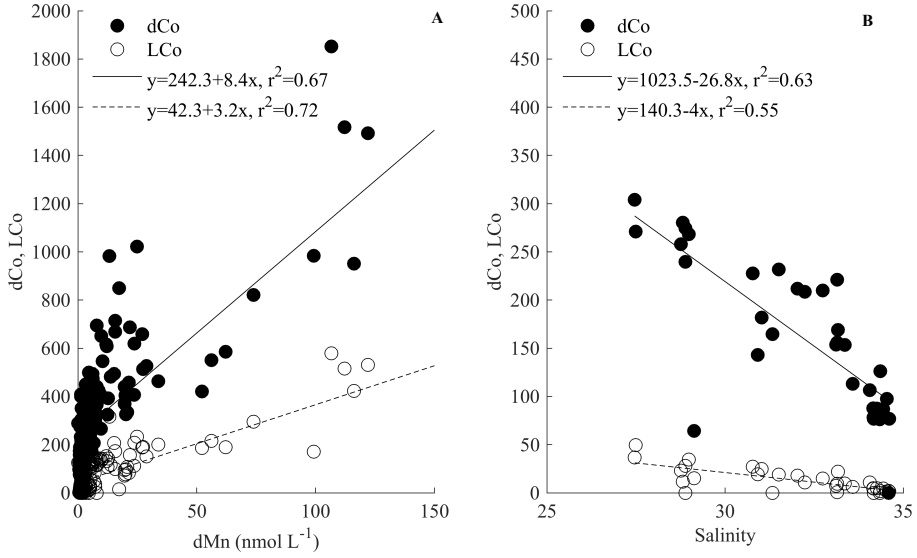

https://doi.org/10.5194/bg-2020-84
Preprint. Discussion started: 9 April 2020

900 **Figure 12.**

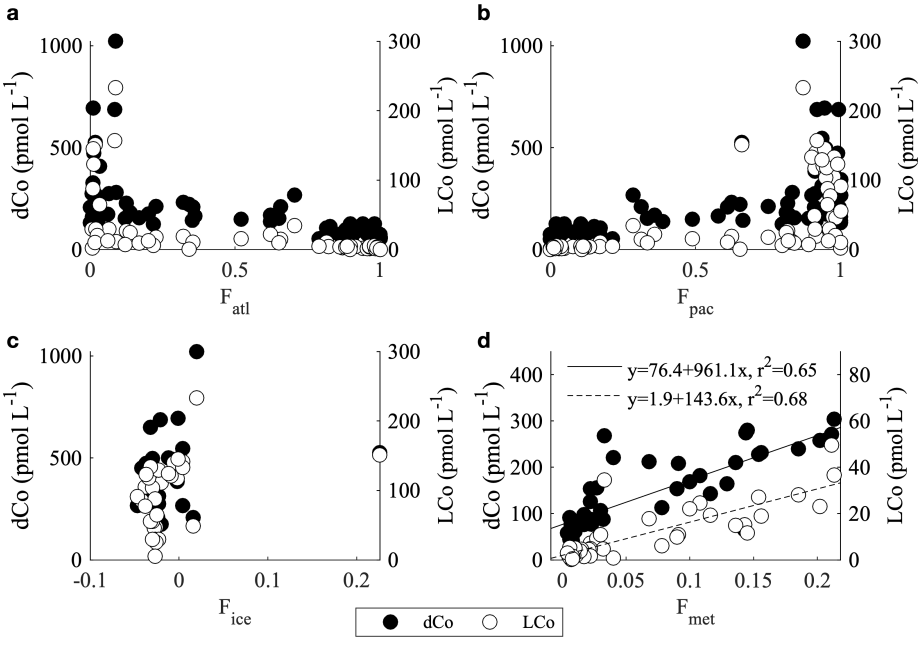

https://doi.org/10.5194/bg-2020-84
Preprint. Discussion started: 9 April 2020

Biogeosciences
Discussions
Open Access
EGU

901 **Figure 13.**

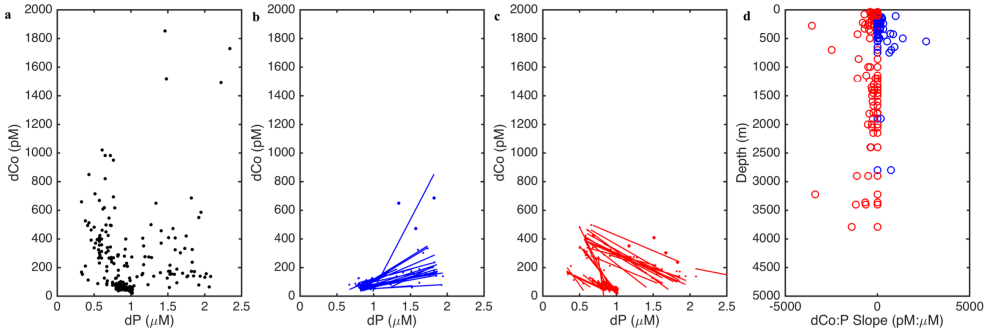

https://doi.org/10.5194/bg-2020-84
Preprint. Discussion started: 9 April 2020

902 **Figure 14.**

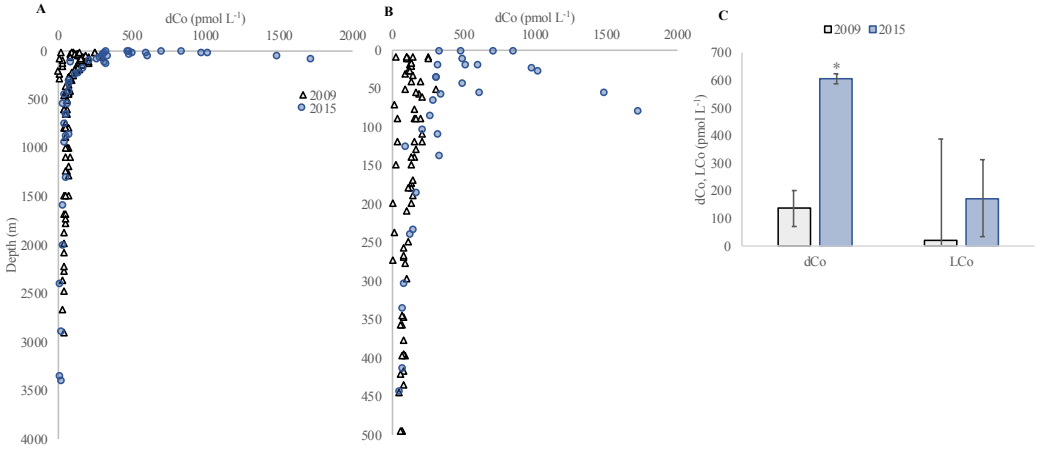

https://doi.org/10.5194/bg-2020-84
Preprint. Discussion started: 9 April 2020

903 **Figure 15.**

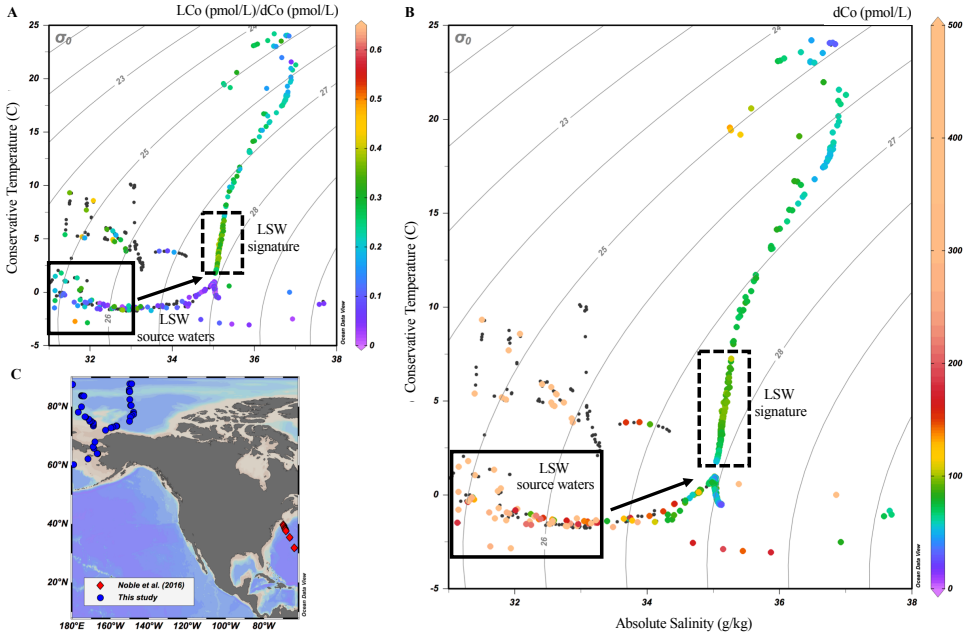

https://doi.org/10.5194/bg-2020-84
Preprint. Discussion started: 9 April 2020

Biogeosciences
Discussions
Open Access
EGU

904 **Figure 16.**

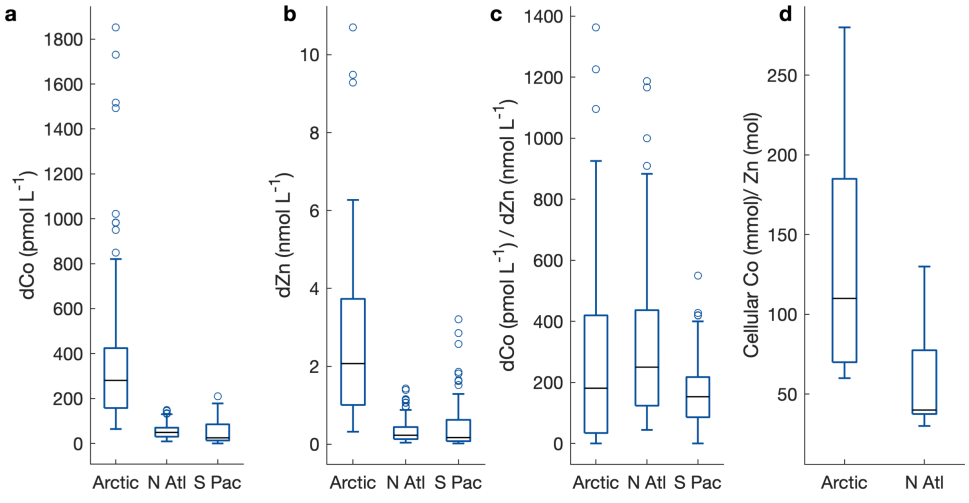

https://doi.org/10.5194/bg-2020-84
Preprint. Discussion started: 9 April 2020

References

Aagaard, K. and Carmack, E. C.: The role of sea ice and other fresh water in the Arctic circulation, J. Geophys. Res. Ocean., 94(C10), 14485–14498, 1989.

Aumont, O., Van Hulten, M., Roy-Barman, M., Dutay, J.-C., Éthé, C. and Gehlen, M.: Variable reactivity of particulate organic matter in a global ocean biogeochemical model, 2017.

Baars, O. and Croot, P. L.: Dissolved cobalt speciation and reactivity in the eastern tropical North Atlantic, Mar. Chem., 173, 310–319, doi:10.1016/j.marchem.2014.10.006, 2015.

Bauch, D., Erlenkeuser, H. and Andersen, N.: Water mass processes on Arctic shelves as revealed from δ18O of H2O, Glob. Planet. Change, 48(1–3), 165–174, 2005.

Bertrand, E. M., Saito, M. A., Rose, J. M., Riesselman, C. R., Lohan, M. C., Noble, A. E., Lee, P. A. and DiTullio, G. R.: Vitamin B $_{12}$ and iron colimitation of phytoplankton growth in the Ross Sea, Limnol. Oceanogr., 52(3), 1079–1093, doi:10.4319/lo.2007.52.3.1079, 2007.

Bertrand, E. M., Allen, A. E., Dupont, C. L., Norden-Krichmar, T. M., Bai, J., Valas, R. E. and Saito, M. A.: Influence of cobalamin scarcity on diatom molecular physiology and identification of a cobalamin acquisition protein, Proc. Natl. Acad. Sci., 109(26), E1762–E1771, doi:10.1073/pnas.1201731109, 2012.

Bertrand, E. M., McCrow, J. P., Moustafa, A., Zheng, H., McQuaid, J. B., Delmont, T. O., Post, A. F., Sipler, R. E., Spackeen, J. L. and Xu, K.: Phytoplankton–bacterial interactions mediate micronutrient colimitation at the coastal Antarctic sea ice edge, Proc. Natl. Acad. Sci., 112(32), 9938–9943, 2015.

Bown, J., Boye, M., Baker, A., Duvieilbourg, E., Lacan, F., Le Moigne, F., Planchon, F., Speich, S. and Nelson, D. M.: The biogeochemical cycle of dissolved cobalt in the Atlantic and the Southern Ocean south off the coast of South Africa, Mar. Chem., 126(1–4), 193–206, 2011.

Le Bras, I. A., Yashayaev, I. and Toole, J. M.: Tracking Labrador Sea water property signals along the deep western boundary current, J. Geophys. Res. Ocean., 122(7), 5348–5366, 2017.

Browning, T. J., Achterberg, E. P., Rapp, I., Engel, A., Bertrand, E. M., Tagliabue, A. and Moore, C. M.: Nutrient co-limitation at the boundary of an oceanic gyre, Nature, 551(7679), 242–246, doi:10.1038/nature24063, 2017.

Bundy, R. M., Abdulla, H. A. N. N., Hatcher, P. G., Biller, D. V., Buck, K. N. and Barbeau, K. A.: Iron-binding ligands and humic substances in the San Francisco Bay estuary and estuarine-influenced shelf regions of coastal California, Mar. Chem., 173, 183–194, doi:10.1016/j.marchem.2014.11.005, 2015.

Carmack, E. C., Macdonald, R. W., Perkin, R. G., McLaughlin, F. A. and Pearson, R. J.: Evidence for warming of Atlantic water in the southern Canadian Basin of the Arctic Ocean: Results from the Larsen-93 expedition, Geophys. Res. Lett., 22(9), 1061–1064, 1995.

Cooper, L. W., Whitledge, T. E., Grebmeier, J. M. and Weingartner, T.: The nutrient, salinity, and stable oxygen isotope composition of Bering and Chukchi Seas waters in and near the Bering Strait, J. Geophys. Res. Ocean., 102(C6), 12563–12573, 1997.

Cooper, L. W., Benner, R., McClelland, J. W., Peterson, B. J., Holmes, R. M., Raymond, P. A., Hansell, D. A., Grebmeier, J. M. and Codispoti, L. A.: Linkages among runoff, dissolved organic carbon, and the stable oxygen isotope composition of seawater and other water mass indicators in the Arctic Ocean, J. Geophys. Res. Biogeosciences, 110(G2), 2005.

Cottrell, M. T. and Kirchman, D. L.: Photoheterotrophic microbes in the Arctic Ocean in summer and winter, Appl. Environ. Microbiol., 75(15), 4958–4966, 2009.

Cowen, J. P. and Bruland, K. W.: Metal deposits associated with bacteria: implications for Fe and Mn marine biogeochemistry, Deep Sea Res. Part A. Oceanogr. Res. Pap., 32(3), 253–272,

https://doi.org/10.5194/bg-2020-84
Preprint. Discussion started: 9 April 2020

1985.
Cutter, G. A. and Bruland, K. W.: Rapid and noncontaminating sampling system for trace elements in global ocean surveys, Limnol. Oceanogr. Methods, 10(JUNE), 425–436, doi:10.4319/lom.2012.10.425, 2012.
Doxaran, D., Devred, E. and Babin, M.: A 50% increase in the mass of terrestrial particles delivered by the Mackenzie River into the Beaufort Sea (Canadian Arctic Ocean) over the last 10 years, 2015.
Doxey, A. C., Kurtz, D. A., Lynch, M. D. J., Sauder, L. A. and Neufeld, J. D.: Aquatic metagenomes implicate Thaumarchaeota in global cobalamin production, ISME J., 9(2), 461, 2015.
Drake, T. W., Tank, S. E., Zhulidov, A. V, Holmes, R. M., Gurtovaya, T. and Spencer, R. G. M.: Increasing alkalinity export from large Russian Arctic rivers, Environ. Sci. Technol., 52(15), 8302–8308, 2018.
Dulaquais, G., Boye, M., Middag, R., Owens, S., Puigcorbé, V., Buesseler, K. O., Masqué, P., de Baar, H. J. W. and Carton, X.: Contrasting biochemical cycles of cobalt in the surface western Atlantic ocean, Global Biogeochem. Cycles, 28, 1387–1412, doi:10.1002/2014GB004903.Received, 2014a.
Dulaquais, G., Boye, M., Rijkenberg, M. J. A. and Carton, X.: Physical and remineralization processes govern the cobalt distribution in the deep western Atlantic Ocean, Biogeosciences, 11(6), 1561–1580, doi:10.5194/bg-11-1561-2014, 2014b.
Dulaquais, G., Planquette, H., L'Helguen, S., Rijkenberg, M. J. A. and Boye, M.: The biogeochemistry of cobalt in the Mediterranean Sea, Global Biogeochem. Cycles, 31(2), 377–399, doi:10.1002/2016GB005478, 2017.
Gascard, J., Festy, J., le Goff, H., Weber, M., Bruemmer, B., Offermann, M., Doble, M., Wadhams, P., Forsberg, R. and Hanson, S.: Exploring Arctic transpolar drift during dramatic sea ice retreat, Eos, Trans. Am. Geophys. Union, 89(3), 21–22, 2008.
Hawco, N. J. and Saito, M. A.: Competitive inhibition of cobalt uptake by zinc and manganese in a pacific Prochlorococcus strain: Insights into metal homeostasis in a streamlined oligotrophic cyanobacterium, Limnol. Oceanogr., 63(5), 2229–2249, 2018.
Hawco, N. J., Ohnemus, D. C., Resing, J. A., Twining, B. S. and Saito, M. A.: A dissolved cobalt plume in the oxygen minimum zone of the eastern tropical South Pacific, Biogeosciences, 13(20), 5697–5717, doi:10.5194/bg-13-5697-2016, 2016.
Hawco, N. J., Lam, P. J., Lee, J. M., Ohnemus, D. C., Noble, A. E., Wyatt, N. J., Lohan, M. C. and Saito, M. A.: Cobalt scavenging in the mesopelagic ocean and its influence on global mass balance: Synthesizing water column and sedimentary fluxes, Mar. Chem., 201(March 2017), 151–166, doi:10.1016/j.marchem.2017.09.001, 2018.
Heal, K.: The Power and Promise of Direct Measurements of Metabolites in Marine Systems, 2018.
Heal, K. R., Qin, W., Ribalet, F., Bertagnolli, A. D., Coyote-Maestas, W., Hmelo, L. R., Moffett, J. W., Devol, A. H., Armbrust, E. V. and Stahl, D. A.: Two distinct pools of B12 analogs reveal community interdependencies in the ocean, Proc. Natl. Acad. Sci., 114(2), 364–369, 2017.
Holmes, R. M., McClelland, J. W., Tank, S. E., Spencer, R. G. . and Shiklomanov, A. I.: Arctic Great Rivers Observatory Water Quality Dataset. [online] Available from: https://www.arcticgreatrivers.org/data, 2018.
Johannessen, O. M., Bengtsson, L., Miles, M. W., Kuzmina, S. I., Semenov, V. A., Alekseev, G. V, Nagurnyi, A. P., Zakharov, V. F., Bobylev, L. P. and Pettersson, L. H.: Arctic climate change:

https://doi.org/10.5194/bg-2020-84
Preprint. Discussion started: 9 April 2020

observed and modelled temperature and sea-ice variability, Tellus A Dyn. Meteorol. Oceanogr., 56(4), 328–341, 2004.
Johnson, K. S., Berelson, W. M., Coale, K. H., Coley, T. L., Elrod, V. A., Fairey, W. R., Iams, H. D., Kilgore, T. E. and Nowicki, J. L.: Mangense flux from continental-margin sediments in a transect through the oxygen minimum, Science (80-.)., 257(5074), 1242–1245, doi:10.1126/science.257.5074.1242, 1992.
Jorgenson, M. T., Shur, Y. L. and Pullman, E. R.: Abrupt increase in permafrost degradation in Arctic Alaska, Geophys. Res. Lett., 33(2), 2006.
Kipp, L. E., Charette, M. A., Moore, W. S., Henderson, P. B. and Rigor, I. G.: Increased fluxes of shelf-derived materials to the central Arctic Ocean, Sci. Adv., 4(1), eaao1302, 2018.
Klunder, M. B., Bauch, D., Laan, P., de Baar, H. J. W., van Heuven, S. and Ober, S.: Dissolved iron in the Arctic shelf seas and surface waters of the central Arctic Ocean: Impact of Arctic river water and ice-melt, J. Geophys. Res., 117, 18, doi:C01027 10.1029/2011jc007133, 2012.
Lane, T. W. and Morel, F. M. M.: Regulation of carbonic anhydrase expression by zinc, cobalt, and carbon dioxide in the marine diatom Thalassiosira weissflogii, Plant Physiol., 123(1), 345–352, 2000.
Lee, J.-M., Heller, M. I. and Lam, P. J.: Size distribution of particulate trace elements in the US GEOTRACES Eastern Pacific Zonal Transect (GP16), Mar. Chem., 201, 108–123, 2018.
Lionheart, R.: Exploring the ocean microbiome: quantified cobalamin production in pelagic bacteria using liquid chromatography and mass spectrometry, 2017.
van der Loeff, M., Kipp, L., Charette, M. A., Moore, W. S., Black, E., Stimac, I., Charkin, A., Bauch, D., Valk, O., Karcher, M. and others: Radium isotopes across the Arctic Ocean show time scales of water mass ventilation and increasing shelf inputs, J. Geophys. Res. Ocean., 123(7), 4853–4873, 2018.
Marsay, C. M., Aguilar-Islas, A., Fitzsimmons, J. N., Hatta, M., Jensen, L. T., John, S. G., Kadko, D., Landing, W. M., Lanning, N. T., Morton, P. L., Pasqualini, A., Rauschenberg, S., Sherrell, R. M., Shiller, A. M., Twining, B. S., Whitmore, L. M., Zhang, R., Buck, C. S. and others: Dissolved and particulate trace elements in late summer Arctic melt ponds, Mar. Chem., 204(June), 70–85, doi:10.1016/j.marchem.2018.06.002, 2018.
Martin, J. H., Gordon, R. M., Fitzwater, S. and Broenkow, W. W.: VERTEX: phytoplankton/iron studies in the Gulf of Alaska, Deep Sea Res. Part A. Oceanogr. Res. Pap., 36(5), 649–680, 1989.
März, C., Stratmann, A., Matthiessen, J., Meinhardt, A. K., Eckert, S., Schnetger, B., Vogt, C., Stein, R. and Brumsack, H. J.: Manganese-rich brown layers in Arctic Ocean sediments: Composition, formation mechanisms, and diagenetic overprint, Geochim. Cosmochim. Acta, 75(23), 7668–7687, doi:10.1016/j.gca.2011.09.046, 2011.
McManus, J., Berelson, W. M., Severmann, S., Johnson, K. S., Hammond, D. E., Roy, M. and Coale, K. H.: Benthic manganese fluxes along the Oregon-California continental shelf and slope, Cont. Shelf Res., 43, 71–85, doi:10.1016/j.csr.2012.04.016, 2012.
Moffett, J. W. and Ho, J.: Oxidation of cobalt and manganese in seawater via a common microbially catalyzed pathway, Geochim. Cosmochim. Acta, 60(18), 3415–3424, doi:10.1016/0016-7037(96)00176-7, 1996.
Moore, C. M., Mills, M. M., Arrigo, K. R., Berman-Frank, I., Bopp, L., Boyd, P. W., Galbraith, E. D., Geider, R. J., Guieu, C., Jaccard, S. L., Jickells, T. D., La Roche, J., Lenton, T. M., Mahowald, N. M., Marañón, E., Marinov, I., Moore, J. K., Nakatsuka, T., Oschlies, A., Saito, M. A., Thingstad, T. F., Tsuda, A., Ulloa, O., Maranon, E., Marinov, I., Moore, J. K., Nakatsuka, T., Oschlies, A., Saito, M. A., Thingstad, T. F., Tsuda, A. and Ulloa, O.: Processes and patterns of

https://doi.org/10.5194/bg-2020-84
Preprint. Discussion started: 9 April 2020

oceanic nutrient limitation, Nat. Geosci., 6(9), 701–710, doi:10.1038/ngeo1765, 2013.
Noble, A. E.: Influences on the oceanic biogeochemical cycling of the hybrid-type metals, cobalt, iron, and manganese, Massachusetts Institute of Technology., 2012.
Noble, A. E., Saito, M. A., Maiti, K. and Benitez-Nelson, C. R.: Cobalt, manganese, and iron near the Hawaiian Islands: A potential concentrating mechanism for cobalt within a cyclonic eddy and implications for the hybrid-type trace metals, Deep Sea Res. Part II Top. Stud. Oceanogr., 55(10–13), 1473–1490, 2008.
Noble, A. E., Ohnemus, D. C., Hawco, N. J., Lam, P. J. and Saito, M. A.: Coastal sources, sinks and strong organic complexation of dissolved cobalt within the US North Atlantic GEOTRACES transect GA03, Biogeosciences, 14(11), 2715–2739, doi:10.5194/bg-14-2715-2017, 2016.
Noble, A. E. A. E., Lamborg, C. H., Ohnemus, D. C., Lam, P. J., Goepfert, T. J., Measures, C. I., Frame, C. H., Casciotti, K. L., DiTullio, G. R., Jennings, J. and Saito, M. A.: Basin-scale inputs of cobalt, iron, and manganese from the Benguela-Angola front to the South Atlantic Ocean, Limnol. Oceanogr., 57(4), 989–1010, doi:10.4319/lo.2012.57.4.0989, 2012.
Resing, J. A. and Mottl, M. J.: Determination of manganese in seawater using flow injection analysis with on-line preconcentration and spectrophotometric detection, Anal. Chem., 64(22), 2682–2687, 1992.
Saito, M. A. and Moffett, J. W.: Complexation of cobalt by natural organic ligands in the Sargasso Sea as determined by a new high-sensitivity electrochemical cobalt speciation method suitable for open ocean work, Mar. Chem., 75(1–2), 49–68, doi:10.1016/s0304-4203(01)00025-1, 2001a.
Saito, M. A. and Moffett, J. W.: Complexation of cobalt by natural organic ligands in the Sargasso Sea as determined by a new high-sensitivity electrochemical cobalt speciation method suitable for open ocean work, Mar. Chem., 75(1–2), 49–68, doi:10.1016/s0304-4203(01)00025-1, 2001b.
Saito, M. A., Moffett, J. W., Chisholm, S. W. and Waterbury, J. B.: Cobalt limitation and uptake in Prochlorococcus, Limnol. Oceanogr., 47(6), 1629–1636, 2002.
Saito, M. A., Moffett, J. W. and DiTullio, G. R.: Cobalt and nickel in the Peru upwelling region: A major flux of labile cobalt utilized as a micronutrient, Global Biogeochem. Cycles, 18(4), 1–14, doi:10.1029/2003GB002216, 2004.
Saito, M. A., Rocap, G. and Moffett, J. W.: Production of cobalt binding ligands in a Synechococcus feature at the Costa Rica upwelling dome, Limnol. Oceanogr., 50(1), 279–290, 2005.
Saito, M. A., Goepfert, T. J., Noble, A. E., Bertrand, E. M., Sedwick, P. N. and DiTullio, G. R.: A seasonal study of dissolved cobalt in the Ross Sea, Antarctica: micronutrient behavior, absence of scavenging, and relationships with Zn, Cd, and P, Biogeosciences, 7(12), 4059–4082, doi:10.5194/bg-7-4059-2010, 2010.
Saito, M. A., Noble, A. E., Hawco, N., Twining, B. S., Ohnemus, D. C., John, S. G., Lam, P., Conway, T. M., Johnson, R., Moran, D. and McIlvin, M.: The acceleration of dissolved cobalt's ecological stoichiometry due to biological uptake, remineralization, and scavenging in the Atlantic Ocean, Biogeosciences, 14(20), 4637–4662, doi:10.5194/bg-14-4637-2017, 2017.
Screen, J. A. and Simmonds, I.: The central role of diminishing sea ice in recent Arctic temperature amplification, Nature, 464(7293), 1334, 2010.
Serreze, M. C. and Barry, R. G.: Processes and impacts of Arctic amplification: A research synthesis, Glob. Planet. Change, 77(1–2), 85–96, 2011.
Shelley, R. U., Sedwick, P. N., Bibby, T. S., Cabedo-Sanz, P., Church, T. M., Johnson, R. J.,

https://doi.org/10.5194/bg-2020-84
Preprint. Discussion started: 9 April 2020

1089 Macey, A. I., Marsay, C. M., Sholkovitz, E. R. and Ussher, S. J.: Controls on dissolved cobalt in
1090 surface waters of the Sargasso Sea: Comparisons with iron and aluminum, Global Biogeochem.
1091 Cycles, 26(2), 2012.
1092 Steele, M. and Boyd, T.: Retreat of the cold halocline layer in the Arctic Ocean, J. Geophys. Res.
1093 Ocean., 103(C5), 10419–10435, 1998.
1094 Steele, M., Morison, J., Ermold, W., Rigor, I., Ortmeyer, M. and Shimada, K.: Circulation of
1095 summer Pacific halocline water in the Arctic Ocean, J. Geophys. Res. Ocean., 109(C2), 2004.
1096 Stroeve, J. C., Serreze, M. C., Holland, M. M., Kay, J. E., Malanik, J. and Barrett, A. P.: The
1097 Arctic's rapidly shrinking sea ice cover: a research synthesis, Clim. Change, 110(3–4), 1005–
1098 1027, 2012.
1099 Sunda, W. G. and Huntsman, S. A.: Effect of sunlight on redox cycles of manganese in the
1100 southwestern Sargasso Sea, Deep Sea Res. Part A. Oceanogr. Res. Pap., 35(8), 1297–1317, 1988.
1101 Sunda, W. G. and Huntsman, S. A.: Cobalt and zinc interreplacement in marine phytoplankton:
1102 biological and geochemical implications, Limnol. Oceanogr., 40(8), 1404–1417, 1995.
1103 Swift, J. H., Takahashi, T. and Livingston, H. D.: The contribution of the Greenland and Barents
1104 seas to the deep water of the Arctic Ocean, J. Geophys. Res. Ocean., 88(C10), 5981–5986, 1983.
1105 Tagliabue, A., Hawco, N. J. N. J., Bundy, R. M. R. M., Landing, W. M. W. M., Milne, A.,
1106 Morton, P. L. P. L. and Saito, M. A. M. A.: The role of external inputs and internal cycling in
1107 shaping the global ocean cobalt distribution: insights from the first cobalt biogeochemical model,
1108 Global Biogeochem. Cycles, 32(4), 1–23, doi:10.1002/2017GB005830, 2018.
1109 Tank, S. E., Striegl, R. G., McClelland, J. W. and Kokelj, S. V: Multi-decadal increases in
1110 dissolved organic carbon and alkalinity flux from the Mackenzie drainage basin to the Arctic
1111 Ocean, Environ. Res. Lett., 11(5), 54015, 2016.
1112 Tebo, B. M., Bargar, J. R., Clement, B. G., Dick, G. J., Murray, K. J., Parker, D., Verity, R. and
1113 Webb, S. M.: Biogenic manganese oxides: properties and mechanisms of formation, Annu. Rev.
1114 Earth Planet. Sci., 32, 287–328, 2004.
1115 Thuróczy, C. E., Boye, M. and Losno, R.: Dissolution of cobalt and zinc from natural and
1116 anthropogenic dusts in seawater, Biogeosciences, 7, 1927–1936, 2010.
1117 Toohey, R. C., Herman-Mercer, N. M., Schuster, P. F., Mutter, E. A. and Koch, J. C.:
1118 Multidecadal increases in the Yukon River Basin of chemical fluxes as indicators of changing
1119 flowpaths, groundwater, and permafrost, Geophys. Res. Lett., 43(23), 12–120, 2016.
1120 Tovar-Sánchez, A., Sañudo-Wilhelmy, S. A. and Flegal, A. R.: Temporal and spatial variations
1121 in the biogeochemical cycling of cobalt in two urban estuaries: Hudson River Estuary and San
1122 Francisco Bay, Estuar. Coast. Shelf Sci., 60(4), 717–728, 2004.
1123 Twining, B. S., Rauschenberg, S., Morton, P. L., Ohnemus, D. C. and Lam, P. J.: Comparison of
1124 particulate trace element concentrations in the North Atlantic Ocean as determined with discrete
1125 bottle sampling and in situ pumping, Deep. Res. Part II Top. Stud. Oceanogr., 116, 273–282,
1126 doi:10.1016/j.dsr2.2014.11.005, 2015.
1127 Twining, B. S., Morton, P. L. and Salters, V. J.: Trace element concentrations (labile and total
1128 measurements) in particles collected with GO-Flo bottles and analyzed with ICP-MS from the
1129 US GEOTRACES Arctic cruise (HLY1502; GNo1) from August to October 2015., Biol. Chem.
1130 Oceanogr. Data Manag. Off., (2019-07–02), doi:10.1575/1912/bco-dmo.771474.2, 2019.
1131 Del Vecchio, R. and Blough, N. V: On the origin of the optical properties of humic substances,
1132 Environ. Sci. Technol., 38(14), 3885–3891, 2004.
1133 Waleron, M., Waleron, K., Vincent, W. F. and Wilmotte, A.: Allochthonous inputs of riverine
1134 picocyanobacteria to coastal waters in the Arctic Ocean, FEMS Microbiol. Ecol., 59(2), 356–

https://doi.org/10.5194/bg-2020-84
Preprint. Discussion started: 9 April 2020

365, 2007.
Wheeler, P. A., Watkins, J. M. and Hansing, R. L.: Nutrients, organic carbon and organic nitrogen in the upper water column of the Arctic Ocean: implications for the sources of dissolved organic carbon, Deep Sea Res. Part II Top. Stud. Oceanogr., 44(8), 1571–1592, 1997.
Yang, R. J. and Van Den Berg, C. M. G.: Metal Complexation by Humic Substances in Seawater, Environ. Sci. Technol., 43(19), 7192–7197, doi:10.1021/es900173w, 2009.
Yee, D. and Morel, F. M. M.: In vivo substitution of zinc by cobalt in carbonic anhydrase of a marine diatom, Limnol. Oceanogr., 41(3), 573–577, 1996.
Zakhia, F., Jungblut, A.-D., Taton, A., Vincent, W. F. and Wilmotte, A.: Cyanobacteria in cold ecosystems, in Psychrophiles: from biodiversity to biotechnology, pp. 121–135, Springer., 2008.
Zhang, H., Van Den Berg, C. M. G. and Wollast, R.: The determination of interactions of cobalt (II) with organic compounds in seawater using cathodic stripping voltammetry, Mar. Chem., 28(4), 285–300, 1990.
Zhang, Y., Rodionov, D. A., Gelfand, M. S. and Gladyshev, V. N.: Comparative genomic analyses of nickel, cobalt and vitamin B12 utilization, BMC Genomics, 10(1), 78, 2009.